Evaluation of ionspray tandem mass spectrometry for the detection and identification of DNA adducts

Daniels, Shirland; Blay, Pearl; Boyd, Robert K.; Pleasance, Stephen; Quilliam, Michael A.

Publisher's version / Version de l'éditeur:
https://doi.org/10.4224/23001224
IMB Technical Report, 1992

EVALUATION OF IONSPRAY TANDEM MASS SPECTROMETRY FOR THE DETECTION AND IDENTIFICATION OF DNA ADDUCTS.

**Issued as IMB Technical Report No. 68,
NRCC No. 33802**

June 1992

Report Prepared For:

**Dr. Shirland Daniels,
National Water Research Institute,
Burlington, Ontario L7R 4A6.**

by:

**Pearl Blay, Robert K. Boyd, Stephen Pleasance,
and Michael A. Quilliam,
Analytical Chemistry Section
Institute for Marine Biosciences,
National Research Council,
1411 Oxford Street, Halifax, Nova Scotia B3H 3Z1.**

TABLE OF CONTENTS

EVALUATION OF IONSPRAY TANDEM MASS SPECTROMETRY FOR THE DETECTION AND IDENTIFICATION OF DNA ADDUCTS.

Report on Work Conducted by the Institute for Marine Biosciences, National Research Council, Halifax, on behalf of

Dr. Shirland Daniels, National Water Research Institute, Burlington.

March, 1992.

Background:

A critical event in the expression of the genotoxicity of carcinogens and mutagens is the formation of covalent chemical adducts between these agents and DNA. In order to understand how these compounds induce mutations and cancer, it is important to elucidate the structures of the adducts and to quantitate their rates of formation and excision. It is also possible that through analysis of the damage to genetic material such as DNA the degree of hazard associated with certain chemicals, samples or environments can be determined. This approach is the basis for a rapidly developing field that has been referred to as "molecular epidemiology".

The traditional approach to the detection of adducts is the use of radiolabelled mutagens and carcinogens. This approach is obviously limited to those compounds that are available with ^{3}H or ^{14}C labels. Recently, an alternative approach has been used with increasing frequency. This is the Randerath enzymatic radiolabelling process (*K. Randerath et al., Proc. Natl. Acad. Sci. USA 78, 6126 (1981); Carcinogenesis 3, 1081 (1982); ibid., 5, 231 (1984)*), in which DNA (containing adducts) is enzymatically hydrolyzed to the 3'-nucleotides, then converted to the [^{32}P]-labelled nucleoside- 3',5'-diphosphates by treatment with γ-[^{32}P]-ATP and a nucleotide kinase. Following multi-dimensional chromatography of this mixture on PEI cellulose TLC plates to separate normal nucleotides from the adduct nucleotides, autoradiography of the TLC plate permits the detection and quantitation of the adducts. This method can detect 1 adduct in 10^{8} to 10^{9} normal nucleotides. If standards are available, it is possible to match R_f values with those of adducts from samples and make tentative identifications. There is a real need for sensitive spectroscopic methods to determine structures of the adducts detected by this method.

Another approach to the characterization of the effects of mutagenic agents on DNA is to perform high resolution separations, such as gel electrophoresis or perhaps capillary zone electrophoresis (CZE), on hydrolyzates of standard DNA (e.g., calf thymus DNA) that have been exposed *in vitro* to suspect samples or compounds, along with the appropriate enzymes. High sensitivity detection is the key to the success of this approach. Fluorescence detectors combined with CZE offer good potential, but this is limited to adducts that fluoresce. Further, the degree

of specificity afforded by fluorescence detection is limited even when both excitation and emission wavelengths are controlled.

Mass spectrometry has long been a useful technique for the analysis of nucleic acids. Many modes of ionization have been employed including electron impact (EI), chemical ionization (CI), field desorption (FD), fast atom bombardment (FAB), and thermospray (TSP). However, while most of these techniques provide important structural information (especially when coupled with tandem mass spectrometry), they suffer from either not having the sensitivity necessary for the analysis of trace levels of components derived from small amounts of DNA or the need to use chemical derivatization techniques to increase volatility and decrease thermal lability.

The new ion-spray mass spectrometry (ISP-MS) technique has great promise as a tool for the detection, identification and quantitation of adducts. Besides being very sensitive for polar compounds such as nucleosides and nucleotides, it is easily interfaced with separation techniques such as HPLC and capillary electrophoresis (CE).

The Proposal:

It was originally proposed that a study be conducted over one year with the following **objectives:**

A. To evaluate the suitability of ion-spray mass spectrometry for the identification of DNA adducts.
B. To evaluate the potential of combining HPLC and CE to ion-spray mass spectrometry for the detection of DNA adducts.

The original plan called for the following **milestones:**

1. Acquisition of adduct standards, either through purchase, from friends or through synthesis. The NCI Chemical Carcinogen Reference Standard Repository now has the 3'-nucleotide adducts of benzo[a]pyrene and 5-methylchrysene available for purchase ($4 per nanogram!) as well as precursors that could be used to make adducts *in vitro*.

2. Evaluation of the ion-spray MS/MS of model compounds (nucleosides, nucleotides, and bases) and/or available adduct standards to evaluate whether it is best (in terms of sensitivity and structural information) to hydrolyze the DNA containing the adducts down to nucleotides (*e.g.*, Fig.1b), nucleosides (*e.g.*, Fig.1c) or bases (*e.g.*, Fig.1d), or even to convert the 3'-nucleotides to 3',5'-nucleoside diphosphates (*e.g.*, Fig.1a). (Note that, in the illustrative examples in Figure 1, adduct formation occurs at the exocyclic amino group of guanine. This will not be true of the synthetic adducts studied experimentally in the present work). The latter would be particularly useful since it would facilitate identification of Randerath-detected adducts. It would also be of interest to analyze oligonucleotide adducts since it is sometimes difficult to hydrolyze DNA completely when adducts are present. The ability of ISP-MS to analyze such large molecules

would be a definite asset. Oligonucleotides up to a 14-mer have already been analyzed by ISP-MS at the 200 pmole level.

3. Evaluation of the potential of using the combined techniques of HPLC/ISP-MS and CE/ISP-MS for the analysis of adducts. Again, this would focus on model compounds and standards. If methods were implemented successfully, analyses of adducts prepared by *in vitro* methods may be attempted.

This is a preliminary investigation to determine whether ion-spray mass spectrometry can play a role in the detection and identification of modifications to DNA by mutagenic substances. If this study is successful, further investigations would be required to perform adequately more detailed work such as: (a) evaluation of quantitative aspects; (b) application to a wider range of adduct-types; and (c) application to more difficult problems such as the identification of adducts formed *in vivo*.

In fact, several changes to the original proposal had to be made. The NCI Reference Standard 3'-nucleotide adduct of benzo[a]pyrene (Figure 1b) was ordered, but on arrival was shown by HPLC/UV analysis to have decomposed to several compounds with almost none of the original adduct surviving. Accordingly, other adducts had to be synthesised at NRC (from N-acetoxy-2N-acetylaminofluorene, NA-AAF), and the results presented here are derived from these synthesised adducts. In addition, only very recently has the problem of interfacing CE to ISP/MS in a reliable way, to give reproducible data, been solved; accordingly, the results presented here represent HPLC/ISP/MS/MS experiments only. To set this approach in context, a short essay on LC/MS and CE techniques is attached as **Part A** of this interim report; it is hoped that this account will help the non-specialist appreciate the great advance in analytical biochemistry made possible by this new instrumental technique. The CE and CE/MS experiments on these DNA adducts will be conducted as soon as both instrument and personnel time permit.

A. LIQUID CHROMATOGRAPHY and CAPILLARY ELECTROPHORESIS

with MASS SPECTROMETRY (LC/MS and CE/MS):

THE SCIEX API III SYSTEM WITH IONSPRAY IONIZATION FOR POLAR ANALYTES.

All chemical separatory techniques involve subjecting a chemical mixture to competing physical effects, so that the different components of the mixture reach different compromises between these effects. For example, classical chromatography involves competition between the tendency of the mobile phase to sweep the compounds with it out of the system, and that of the stationary phase to retain the compounds; the different compromises between these two effects result in separation of the different components in time (in the case of column chromatography) or in space (in the case of thin-layer chromatography). Other separatory methods, such as capillary electrophoresis, involve compromises between different competing physical effects, as discussed below.

The importance of analytical chromatography for the separation of complex mixtures (often including isomeric components) lies in its ability to simultaneously provide qualitative analyses (confirmation of compound identity *via* both retention time and signature from some selective detector, *vide infra*) and quantitative analyses (*via* appropriate comparisons with the response from some external or internal standard). **(See Figure 2).** A wide range of analyte types can be dealt with by the complementary methods of high-resolution separatory methods presently available, *viz.* gas chromatography (GC), high performance liquid chromatography (HPLC, or often simply LC), supercritical fluid chromatography (SFC), and capillary electrophoresis (CE, or HPCE, or sometimes CZE). Each of these separatory methods has its own unique combination of advantages and disadvantages, *e.g.* capillary column GC easily provides high resolution separations, but only for compounds which are sufficiently volatile and robust that they can withstand being held in the gas phase for times of up to 1 hour, at temperatures up to 250°C or greater.

Mass spectrometry (MS) currently provides the detection method of choice for analytical chromatography. **(See Figure 3).** Its combination of universal applicability at high sensitivity, together with the selectivity of detection implicit in its provision of both molecular weight information (including elemental composition if conducted at sufficiently high mass resolving power) and structural information (*via* characteristic fragmentations of the gaseous ions which are the sample-derived entities actually detected by MS), is unrivalled by any detector currently available. In order for the electromagnetic fields to separate the gaseous ions according to their mass-to-charge (m/z) ratios, the environment within the MS itself must be maintained at a sufficiently high vacuum that ion-neutral collisions do not perturb the field-induced motions of the ions which provide the basis for the m/z separation. For this reason it is not surprising that, historically, the first ionization methods, electron ionization (EI) and chemical ionization (CI) (see **Figure 4**), involved pre-volatilization of analytes prior to their injection into the MS vacuum

chamber. For the same reasons, GC was the first chromatographic method to be successfully coupled to MS, and GC/MS is now a mature technique in wide use **(see Figure 5).**

The limitation of GC/MS techniques to volatile, thermally robust compounds can be circumvented to some extent by chemical derivatisation, usually of functional groups involved in strong intermolecular hydrogen bonding. However, such methods are time consuming, and can introduce artifacts into the GC/MS datasets which can create confusion. Other shortcomings of GC methods in general, including GC/MS, include the low degree of repeatability of liquid injection volumes (analyte in liquid solution) into the gas stream mobile phase; this is frequently a limiting factor in the overall precision obtainable in quantitative analyses by GC/MS.

Many of these disadvantages of GC do not exist for HPLC **(see Figure 6).** Thus, separations are conducted at or near room temperature in a liquid mobile phase, so that lack of volatility and thermal fragility are no longer a problem. The repeatability of liquid injection volumes into the liquid mobile phase, using modern injection loop technology, is sufficiently high that this is seldom (if ever) the limiting factor in quantitative analyses. Other advantages of HPLC over GC include its amenability to preparative fraction collection for off-line characterization. These advantages come at the price of lower column efficiency than that obtainable using GC, and difficulties in interfacing to MS.

It is possible to use off-line MS analysis of fractions separated by HPLC, but on-line LC/MS is preferable for several reasons **(see Figure 7)** including possibilities for computer-assisted analyses of complex mixtures not fully resolvable by HPLC, quantitative analyses, and savings in time and effort. However, until recently, fundamental problems in interfacing HPLC to MS made combined LC/MS a specialised analytical technique. The most obvious problem **(see Figure 8)** involves the mismatch between the HPLC mobile phase and the vacuum pumping capability of even the best modern MS vacuum systems. The sheer volume of gas generated from the liquid mobile phase (up to 1200 mL/min of gas, measured at atmospheric pressure, from 1 mL/min of liquid) is some 200 times too great for the MS pumping system, and this problem can be exacerbated by the changing mobile phase composition characteristic of gradient elution HPLC. In addition, many mobile phase modifiers (buffers, ion-pairing regents, *etc.*) are insufficiently volatile to be pumped away by vacuum pumps. A less obvious problem involves the wide range of analyte types which are amenable to HPLC methods, which in turn implies a requirement for a wide range of ionization methods in the mass spectrometric stage of LC/MS analyses; for example, EI or CI are desirable ionization methods for thermally robust analytes such as polycyclic aromatic compounds (PAC), but for fragile analytes such as peptides and proteins, or nucleosides and nucleotides, methods such as fast-atom bombardment (FAB) or its variants are required. All of these problems must be solved with no deterioration of chromatographic performance, a daunting task.

Successful methods of interfacing HPLC to MS can be categorized as involving mobile-phase removal, reduction of flow-rate into the mass spectrometer, or special methods combining the interfacing of a liquid effluent to a vacuum chamber with the ionization process itself **(see Figure 9).** The most common method based on mobile phase removal is that provided by the

moving belt interface (see **Figure 10**), which can be used successfully with EI, CI or FAB ionization and is thus applicable to a wide range of compound types; however, the use of FAB ionization with this interface has proved, in practice, to be difficult and far from routine. The particle-beam interface, also involving solvent removal, has been recently introduced for use with EI or CI, but its range of applicability to real-world problems has yet to be established. An alternative approach to the problem of overloading the MS vacuum system, is to reduce the mobile phase flow-rate to values compatible with the pumping capacity. This can be done either by splitting the HPLC effluent from standard analytical HPLC columns (i.d. values 1 - 4.6 mm), diverting the majority of the flow to a complementary detector (*e.g.* UV-visible) or fraction collector, or by using micro-LC columns (i.d. less than 300 microns) with no split. The use of a large split ratio, or of low sample loadings characteristic of micro-LC columns, leads to reduced sensitivity for minor components. Ionization methods used in conjunction with each of these flow-rate reduction strategies include CI with the mobile phase acting as CI reagent gas (direct liquid introduction), and continuous-flow FAB (see **Figure 11**); both methods have considerable problems in practice.

The special combined techniques, in which the transformation of an atmospheric pressure liquid into gas phase ions is accomplished within a single device, include thermospray (TSP) and its variants, and various methods of atmospheric pressure ionization (API). The TSP method (see **Figure 12**) involves heating the liquid effluent just before its introduction to the MS vacuum chamber; the mobile phase thus protects the analyte by absorbing most of the thermal shock, and the rapid expansion of the partially vaporized effluent into the vacuum chamber provides expansion-cooling together with analyte ionization *via* mechanisms which are probably related to the ion-evaporation process discussed below. In practice TSP is a reliable technique for LC/MS, though its efficiency is highly compound-dependent (probably reflecting some residual susceptibility to thermal degradation) and the derived ion currents are highly irreproducible. More recently API methods for LC/MS have been introduced, and these show considerable promise for making LC/MS analyses almost as routine as the well-established GC/MS techniques. The heated pneumatic nebulizer (HPN) bears a superficial resemblance to TSP; however, the heating is much more gentle (about 100°C maximum) and is applied at atmospheric pressure. The nebulised droplets thus drift through a hot atmosphere, permitting rapid evaporation of mobile phase leaving extremely small micro-particles of analyte whose vapour pressure is many times larger than that of the bulk material. The vaporized analyte is then subjected to soft chemical ionization initiated by a corona discharge at atmospheric pressure, and the ions are sampled through a micron-sized orifice, protected by a counter-current of dry nitrogen, into the MS vacuum chamber. This HPN technique can be highly efficient for analytes of moderate volatility and thermal stability, but is not applicable to very large and/or polar analytes.

Fortunately, a complementary API technique is particularly sensitive for just those highly polar analytes unsuited to the HPN interface. This technique presently exists as two variants, electrospray (ESP) and ionspray (ISP); the latter is essentially identical to the former, but with the addition of pneumatic nebulization of the LC effluent. The essential features of both ESP and ISP include operation at room temperature and pressure, and no subsidiary ionization step

such as atmospheric pressure CI initiated by corona discharge. The effluent is pumped through a stainless steel needle maintained at a potential of several kV, and of polarity the same as that of the desired ions (see **Figure 13**). Without pneumatic assistance, electrostatic instabilities at the needle can effect efficient nebulization at flow-rates of up to 5-10 μL/min, but this upper limit can be increased by factors of up to 20 with pneumatic assistance. The nebulised droplets emerging from the charged needle are themselves charged, and drift towards the orifice leading to the MS vacuum under the influence of the resulting Coulombic repulsion. During this drift time the mobile phase is progressively removed into the ambient atmosphere, until the droplets have shrunk to a small enough size that the charge density at the surface renders the droplets electrically unstable. The electrostatic stress is relieved by expelling pre-formed ions from the liquid surface into the surrounding atmosphere. These ions possess much higher mobilities than do the droplets from which they originated, and are accelerated towards the orifice under the influence of the applied fields. The MS is protected from droplets and most of the ambient atmosphere by a counter-current flow of dry nitrogen (gas curtain); even so, extremely efficient vacuum pumps are required, usually cryopumps operating at liquid helium temperatures.

The LC/ISP/MS combination is an extremely powerful tool for analysis of polar compounds which readily produce pre-formed ions in the liquid phase. Although flow-rates of up to 200 μL/min can be accomodated, optimum efficiency generally requires a flow-rate of 50 μL/min or less. This can be achieved using split ratios of about 20:1 and 4:1 for 4.6 mm and 2.1 mm i.d. columns, respectively, or direct connection of 1 mm or 320 μm i.d. columns, under typical operating conditions (see **Figure 14**). The LC/ISP/MS interface introduces no deleterious effects on chromatographic performance relative to that obtainable using a modern UV detector. In positive ion mode the mass spectra are typically dominated by protonated molecules MH^+, with little evidence of fragmentation (see **Figure 15**). While this concentration of ion current, in just one ionic species carrying molecular weight information, is of value for high sensitivity quantitative analyses of target analytes by selected ion monitoring (SIM) techniques, no structural information is available. Use of tandem mass spectrometry (MS/MS) techniques (see **Figure 16**) to fragment these MH^+ ions can, however, fill this gap if required (see **Figure 15**). Quantitation using ionspray ionization is excellent, even though some slight curvature is typically observed in the calibration curves over several orders of magnitude (see **Figure 17**). For analytes amenable to the technique, LC/ISP/MS provides an analytical method with excellent sensitivity, selectivity and reproducibility.

Electrophoresis is a general term applied to the phenomenon of migration of charged molecular species through a solution under the influence of an applied electric field. Several variants of this technique are in common use by biochemists, in order to separate polar biological molecules such as peptides and proteins. For example, an early application of such classical biochemical techniques to PSP toxins involved separation of some of the toxins by cellulose acetate electrophoresis. Work by Dr. Laycock of IMB, associated with his successful isolation of pure PSP toxins (see Section B above), used high-voltage paper electrophoresis to monitor relative amounts of classes of PSP toxins.

Capillary electrophoresis (CE) is a new approach to electrophoresis in which the traditional gel slabs, paper sheets, *etc.*, are replaced by narrow bore (typically 50-100 μm i.d., and approx. 360 μm o.d.) fused silica capillaries of length 50-150 cm. The capillaries are coated on the outside with a thin polyimide film in order to preserve flexibility and mechanical strength. CE accommodates very high voltages (up to 30 kV, giving field strengths up to 600V/cm) and current densities (up to $5A/cm^2$, equivalent to currents of up to 300 μA depending on the nature of the supporting buffer) because of the efficient dissipation of Joule heat made possible by the large ratio of surface area to volume. In turn this efficient cooling results in minimal radial temperature gradients, thus minimising problems associated with convection and variations in viscosity across the capillary cross section. This radial uniformity is the ultimate guarantor of the very high separation efficiencies (up to 10^6 theoretical plates in 20-25 min) achievable using CE. It is not appropriate here to describe in detail the physical principles underlying analytical CE; excellent expositions are available in the literature, (*J.W.Jorgenson, Anal.Chem. 58, 743A-760A (1986); A.G.Ewing, R.A.Wallingford and T.M.Olefirowicz, Anal. Chem,. 61, 292A-303A (1989); P.D. Grossman, Amer. Biotech. Lab., Feb. 1990, pp.35-43*). However, it is worthwhile for present purposes to emphasise that emergence of an analyte from one end of the capillary is the result of the interplay of two competing transport mechanisms. The first of these is the electrophoretic mobility of the charged analyte species through the supporting buffer solution, under the influence of the applied field; this mobility is a function of the size (and possibly shape) of the solvated species, and of its net charge. The second transport mechanism is electroendosmosis, which is the bulk flow of liquid resulting from the effect of the applied field on the electrical double layer adjacent to the capillary wall. Figure 18 illustrates these two effects as a function of pH, for the present case where the net charge on the untreated silica internal wall is negative so that the adjacent double layer carries a net positive charge; this annulus of positive charge is thus drawn towards the negative electrode. The bulk liquid flow that results is the electroendosmotic flow, and is characterised by its flat profile, in contrast to the parabolic profile typical of flow induced by pressure difference (Figure 19); thus the flow profile does not contribute to band broadening, as is the case for HPLC for example. The other important feature of CE is the very low volume flowrate (of the order of 100 nL/min) emerging from the capillary. This fact has implications for development of CE-MS technologies. Figure 20 compares CE-UV and CE-MS results for a mixture of two polar marine toxins. Attached to this report are copies of papers describing the advances in CE-ME methodology made at IMB.

B. LC-UV and LC-MS RESULTS OBTAINED FOR DNA FRAGMENTS.

Over 50 different nucleic acid components were examined by ionspray MS, MS-MS and LC-MS. The development of a reliable CE-MS interface took much longer than hoped, and thus far time has permitted examination of only marine toxins and proteins by this technique (see Section D below). The compounds relevant to this work, examined by MS and LC-MS, included representatives from each of the following classes:

- nucleobases (e.g. guanine G);
- 2' - deoxynucleosides (e.g. dG);
- ribonucleosides (e.g. rG);
- 2' - deoxynucleoside - 5' - monophosphate nucleotides (e.g. pdG);
- 2' - deoxynucleoside - 3' - monophosphate nucleotides (e.g. dGp);
- dinucleoside - monophosphates (e.g. dCpdG);
- cyclic monophosphates of nucleosides;
- synthetic adducts (see Section C below for details) of the carcinogen N-acetoxy-2- N-acetylaminofluorene (NA-AAF);

All of these compounds showed excellent sensitivity in positive-ion ionspray mass spectrometry. The mass spectra are dominated by protonated molecules $(M + H)^+$, and by a fragment ion corresponding to expulsion of the sugar ring (with its phosphate, if present) accompanied by transfer of a hydrogen atom from the sugar moiety to the protonated nucleobase. This yields two even-electron fragments, the unsaturated sugar residue and the ionic fragment $(B+2H)^+$, where B denotes the radical fragment of the DNA base, *e.g.* guanyl. A speculative mechanism for this rearrangement-fragmentation process is shown below:

A few representative spectra follow. In order to keep the number of figures down to a reasonable number, spectra are shown mainly for compounds based on the guanine structure since G is the base most often involved in adduct formation. However, corresponding spectra were also obtained for many compounds incorporating the other nucleobases. In addition, UV spectra were also obtained for many compounds studied, since these can be useful in confirming adduct structures (see below).

A few observations concerning Figures 21 - 30 now follow. The UV-visible spectrum of guanine (Figure 1a) is remarkable only for the fact that it was obtained using a diode array detector (DAD) as an HPLC detector, i.e. the spectrum was obtained as the guanine eluted from an HPLC column. This feature is important since it permits using the UV spectrum as confirmatory identification evidence as components of a mixture elute from the column. Figure 21b is a mass spectrometric fingerprint for guanine; the transition m/z 152 → m/z 135 for protonated guanine corresponds to expulsion of neutral NH_3, most probably originating from the (protonated) exocyclic amino group. The fragment ion at m/z 110 corresponds to expulsion from the $(M+H)^+$ ion of a neutral fragment of molecular weight 42, which must contain an even number of nitrogen atoms if the fragments are to remain in the even-electron category; this neutral fragment is most likely either CH_2N_2 from the 5-membered ring in guanine, or possibly CH_2CO (ketene).

The comparison of the two spectra of N2-acetyl-G, shown in Figure 22, is interesting from a mass spectrometric point of view. Ionspray ionisation usually yields only a $(M+H)^+$ ion from the neutral molecule M. However, it is possible to operate the ionspray interface (specifically, the electrical potential in the "gas-curtain" interface region linking the atmospheric pressure ionisation source to the mass spectrometer vacuum chamber) so that fragmentation is induced by collisions occurring there. Figure 22a illustrates this facility; the collision conditions in the interface region were such that the principal fragmentation reaction was expulsion of the entire (protonated) N2-exocyclic group as the stable neutral CH_3CONH_2 (acetamide). On the other hand, Figure 22b shows the fragment ion spectrum of those $(M+H)^+$ ions (m/z 194) which survived the interface region and which were subsequently collisionally activated in the MS-MS collision cell of the SCIEX API III instrument (see Figure 16). In this case the gentler collision conditions led predominantly to expulsion of the stable neutral species CH_2CO (ketene), leaving the ion at m/z 152 (presumably protonated G) as the most intense fragment ion although a weak signal at m/z 135 can also be seen in Figure 22b.

Figure 23 shows spectral data for dG. The UV spectrum shown in Figure 23a is very similar to that of G itself (Figure 22a), as expected from the fact that the main chromophore in this wavelength range is the purine ring system (the deoxyribose in dG is expected to affect the spectrum only via secondary effects such as steric interactions). The ionspray mass spectrum of dG (Figure 23b) shows an intense $(M+H)^+$ ion at m/z 268, but also an equally intense fragment ion at m/z 152 corresponding to the $(M+H)^+$ ion of the bare G base. The latter identification is supported by Figure 23d, which shows an MS-MS spectrum of those fragments at m/z 152 which survived extraction through the ionspray interface region; Figure 23d is closely similar to Figure 21b, which is the corresponding spectrum obtained for m/z 152 formed

directly as $(M+H)^+$ ions of guanine itself. Figure 23c is the MS-MS spectrum for protonated dG (m/z 268), and shows the expected protonated-G fragment $(B+2H)^+$ at m/z 152 as well as a fragment ion at m/z 117 which corresponds to protonated deoxyribose. Once again, the difference between the fragment ions observed in Figures 23b and 23c illustrates the difference between dissociations induced by collisions occurring in the interface region and those in the quadrupole collision cell (Figure 16).

Figure 24 is the ionspray mass spectrum of riboguanine (rG), showing the $(M+H)^+$ ion at m/z 284 (16 m/z units higher than that of dG, Figure 23b, as predicted), and the same fragment ion at m/z 152 corresponding to protonated G base. (The ion at m/z 306 corresponds to the $(M+Na^+)$ ion of rG, arising from residual Na^+ ion in the sample as received from the supplier). Figure 25 shows the ionspray mass spectrum of deoxyadenosine (dA), which shows features entirely analogous to those for dG in Figure 23b, including the $(A+H)^+$ ion at m/z 136.

Figure 26 shows illustrative spectra for isomeric nucleotides (guanosine monophosphates). Figure 26a shows the UV spectrum of pdG; this spectrum is still recognisable as a distorted version of that of underivatised G (Figure 21a). The ionspray mass spectrum of pdG (Figure 26b) shows the anticipated $(M+H)^+$ and $(M+Na)^+$ ions at m/z 348 and 370, respectively, and also the now-familiar fragment ions at m/z 152 (protonated G) and m/z 135 (loss of neutral NH_3 from protonated G). The different collision conditions in the MS-MS collision cell induce different fragmentation reactions of the $(M+H)^+$ ion of pdG, as shown in Figure 26c; protonated guanine (m/z 152) is still the dominant fragment ion, with no evidence for the accompanying m/z 135 (Figure 26b), but now the fragment ion at m/z 81 is attributable to the $H_2PO_3^+$ cation. This fragment ion is absent from the MS-MS spectrum (Figure 26d) of the $(M+H)^+$ ion of the isomeric nucleotide dGp (3'-monophosphate); this difference could offer a means of distinguishing between 3'- and 5'-sugar-phosphate linkages in such mononucleotides.

Figures 27 and 28 compare the MS-MS spectra of the $(M+H)^+$ ions of a N2-derivatised nucleoside (N2-isobutyryl-dG) and of the corresponding nucleotide, 5'-monophosphate (N2-isobutyryl-pdG). In each case the most intense fragment ion is the protonated derivatised base (N2-isobutyrylguanine, $(M+H)^+$ at m/z 222). In the case of the nucleoside (Figure 27) fragment ions at m/z 152 and 117 correspond to protonated guanine and protonated deoxyribose, respectively. These latter fragments are absent from the MS-MS spectrum of the corresponding nucleotide (Figure 28), but again the $H_2PO_3^+$ ion at m/z 81 arises from the 5'-monophosphate group (compare Figure 26c).

Finally, Figures 29 and 30 illustrate ionspray mass spectra obtained from two dinucleotides. In both cases the $(M+H)^+$ and $(M+Na)^+$ ions are observed, at m/z 541 and 563 in Figure 29 for dApdC, and at m/z 581 and 603 in Figure 30 for dApdG. However, the fragmentation characteristics are somewhat different in these two spectra, which were obtained under identical experimental conditions. In the case of dApdC (Figure 29) fragment ions corresponding to both protonated bases are observed, at m/z 136 for $(A+H)^+$ and at m/z 112 for $(C+H)^+$; the ion at m/z 430 corresponds to expulsion of neutral intact C from the $(M+H)^+$ ion at m/z 541. In contrast, the dApdG (Figure 30) shows only one fragment ion at m/z 136.

C. PREPARATION OF SYNTHETIC ADDUCTS; SPECTRAL PROPERTIES.

The adducts of N-acetoxy-2N-acetylaminofluorene (NA-AAF), with each of 2'-deoxyguanosine (dG) and 2'-deoxyguanosine-5'-monophosphate (pdG), were prepared following the procedure of *E. Kriek et al., Biochemistry 6, 177 (1967)*. These reactions involve the C8 position of the purine ring, rather than the exocyclic amino group involved in the benzpyrene adducts illustrated in Figure 1. Additional reactions were also conducted to transform the initial dG^{AAF} and pdG^{AAF} adducts (Figure 31) into related compounds which could be formed by controlled hydrolysis of DNA. Thus, treatment with dilute acid successfully hydrolysed off the sugar residue, to leave the AAF adducts of guanine itself (G^{AAF}, Figure 31); further treatment with concentrated HCL hydrolysed the N-acetoxyl bond to yield the G^{AF} adduct (Figure 31). Alkaline hydrolysis of the dG^{AAF} adduct has been reported to selectively hydrolyse the N-acetoxyl linkage, leaving intact both the guanine-sugar linkage and the sugar-phosphate linkage, and thus producing the dG^{AF} and pdG^{AF} adducts (Figure 31). However, under these aklaline conditions it was found in the present work that the products formed were due to simultaneous hydroxylation of the fluorene ring (Figure 31); these hydroxylated products dG^{AFOH} and pdG^{AFOH} have apparently not been reported previously in the literature. Some examples of LC-MS analyses of these reaction products are shown in Figures 32-39. Note that, for each of these Figures summarising the LC-MS data, the relative intensities on the vertical scales apply only within that Figure but are not comparable amongst different Figures.

Figure 32 summarises the analytical results for the reaction products of pdG mixed with NA-AAF. The $(M+H)^+$ ion (m/z 569) of the anticipated reaction product pdG^{AAF} (Figure 31) is observed at a retention time of 4.73 min (Figure 32d), with a minor contribution from some isobaric compound at 5.72 min. The latter might be the dGp^{AAF} isomer, arising from an impurity, but no confirmation of this speculation was obtained other than the partially resolved shoulder on the chromatogram for m/z 348 (Figure 32b) which is consistent with a small amount of dGp in the pdG sample. The most intense signal was that obtained for m/z 373 (Figure 32c) at 4.73 min. Although the $(M+H)^+$ ion of G^{AAF} has m/z 373, it is unlikely that pdG^{AAF} and G^{AAF} would have identical retention times (both 4.73 min). It is much more likely that the ion at m/z 373 was formed as a mass spectrometric fragment ion of the $(M + H)^+$ ion of pdG^{AAF} (see Figure 41) *via* expulsion of the sugar-phosphate moiety (with transfer of a hydrogen atom to the guanine base to preserve the even-electron character). The small peak at 7.15 min (Figure 32c), however, does correspond to G^{AAF} in the reaction mixture. The null channel (m/z 331, Figure 32a) was generated in error.

The corresponding LC-MS data for the reaction products of NA-AAF plus dG are summarised in Figure 33. The $(M+H)^+$ ion of the anticipated product dG^{AAF} (m/z 489) shows up at 6.90 min. As in Figure 32, the m/z 373 ion is much more intense and has an elution profile which is superimposable upon that for m/z 489. Again, this strongly suggests that the ion at m/z 373 is formed as a fragment ion of that at m/z 489 (due to collisions in the ionspray interface region), and does not in this case correspond to the $(M+H)^+$ ion of a reaction side-product G^{AAF}. Confirmation that such fragmentations were occuring can be found in the signals in the channels for m/z 268 (Figure 33a, $(M+H)^+$ ion for dG) and for m/z 331 (Figure 33b,

$(M+H)^+$ ion for G^{AF}), both of which also co-elute with m/z 489. The intense peak at 2.85 min in Figure 33a represents unreacted dG.

As mentioned above, hydrolysis by dilute acid of these adducts is anticipated to preferentially hydrolyse the base-sugar linkage. Figure 34 summarises the results of LC-MS analysis of the dG^{AAF} adduct after hydrolysis by 0.05 M HCL. The most intense signal (Figure 34c, m/z 373, 7.12 min) does indeed correspond to the $(M+H)^+$ ion from the anticipated hydrolysis product G^{AAF}. The m/z 331 channel (Figure 34b, $(M+H)^+$ ion from G^{AF}) shows a weak signal also at 7.12 min attributable to a fragment ion of m/z 373 (loss of CH_2CO, ketene), but also an intense signal at 5.50 min which must correspond to the $(M+H)^+$ ion of G^{AF} formed as a side-product (further hydrolysis of the N-acetyl group of G^{AAF}). The sharp peaks at 2.65-2.70 min in Figures 34a and 34d correspond to elution at t_o, and arise from salt clusters and other extraneous species.

Hydrolysis of dG^{AAF} with 1.0 M HCL yielded a reaction mixture whose LC-MS analysis gave results summarised in Figure 35. These results are similar to those obtained for dilute acid hydrolysis (Figure 34), except that the more fully hydrolysed product G^{AF} (m/z 331, Figure 35b) is now more abundant than the partially hydrolysed product G^{AAF} (m/z 373, Figure 35c).

Hydrolysis of the original adducts by alkali was anticipated from the literature to selectively hydrolyse the N-$COCH_3$ linkage, leaving the base-sugar and sugar-phosphate linkages intact (see Figure 31). The reaction product thus predicted for alkaline hydrolysis of pdG^{AAF} is pdG^{AF} , with an $(M+H)^+$ ion at m/z 527. However, the corresponding LC-MS channel (Figure 36c) is empty, apart from the sharp signal at t_o (2.70 - 2.75 min). However, a strong signal in the m/z 543 channel at 4.28 min indicates formation of the hydroxyl derivative pdG^{AFOH}. The weak peak in the m/z 348 channel (Figure 36a) at the same retention time, indicates formation of a fragment ion from m/z 543, with the molecular weight predicted for G^{AFOH}.

Figure 37 summarises LC-MS results for reaction products from the alkaline hydrolysis of dG^{AAF} . The results are entirely analogous to those shown in Figure 36 for alkaline hydrolysis of pdG^{AAF}. Thus, the predicted product dG^{AF} (m/z 447 for $(M+H)^+$) is not observed (Figure 37c), but its hydroxylated derivative dG^{AFOH} (m/z 463) is observed (Figure 37d). Again, m/z 347 (Figure 37a) appears to be formed as a mass spectrometric fragment ion. The extremely strong signals for both m/z 431 and m/z 567, observed at t_o in both Figures 36 and 37, are cluster ions of sodium trifluoroacetate.

Close examination of the LC peak at 4.42 min in Figure 37d suggested the presence of unresolved components. Accordingly, different HPLC conditions (lower methanol content, and thus longer retention times for these reverse-phase separations) were tried. The results thus obtained are summarised in Figures 38 and 39 for the same two-reaction mistures as those used to obtain Figures 36 and 37, respectively. At least three components can now be discerned in the m/z 543 channel (Figure 38c), i.e. that for the $(M+H)^+$ ions from pdG^{AFOH}. The well-resolved peak at 16.02 min might correspond to the isomer dGp^{AFOH}, since other evidence (Figure 32) suggests the possibility of contamination of the pdG sample with a small proportion

of dGp. The LC peak pattern (Figure 38c) is reproduced in Figure 38a (m/z 347), as would be predicted for a mass spectrometric fragmentation relationship between m/z 543 and m/z 347. However, the peak at 18.72 min in Figure 38a does not correspond to any such feature in Figure 38c, and probably arose from a small quantity of G^{AFOH} produced as a side-product in the hydrolysis reaction. The intense signal at t_o, in the m/z 567 channel, is again due to the sodium trifluoroacetate cluster ion. The m/z 463 channel ($(M+H)^+$ ion for dG^{AFOH}) is empty except for the effluent at t_o .

The corresponding results for the alkaline hydrolysis products of dG^{AAF} are summarised in Figure 39. The LC peak in the m/z 436 channel ($(M+H)^+$ ion for dG^{AFOH}) is now well-resolved into two compounds, also reflected in the m/z 347 channel again reflecting a mass spectrometric connectivity relationship. These are presumably isomeric forms of dG^{AFOH}, arising from positional isomerism of the hydroxyl in the fluorene ring (Figure 31), and the same is probably true of the partially-resolved peaks in Figure 38c. Thus, it seems clear that alkaline hydrolysis of adducts such as pdG^{AAF} and dG^{AAF} does indeed hydrolyse the N-acetyl linkage selectively while leaving intact the base-sugar and sugar-phosphate linkages intact, as indicated in the literature. However, the unique LC-MS capabilities available in this work show that this highly selective hydrolysis is accompanied by hydroxylation (presumably of the fluorene ring system to give isomeric phenols).

Spectroscopic data, for some of the key adducts involving guanine, are shown in Figures 40-45. All of these spectra were obtained in on-line HPLC experiments using a diode - array detector and the SCIEX API III mass spectrometer using the ionspray interface. The objective in these experiments was to obtain good quality reference spectra, without concern for sensitivity.

A separate set of experiments was conducted to investigate the sensitivity of the present LC-MS methodology for guanine-based nucleosides and nucleotides, and their NA-AAF adducts. Figure 46 shows results of a preliminary LC-MS analysis of a mixture of six compounds (dG, pdG, G^{AF} , G^{AAF} , dG^{AAF} , and pdG^{AAF}), each at a concentration of approximately 50 μg/mL. The injection volume was 5μL, so approximately 250 ng of each was injected on-column; the 1:20 post-column split implied that approximately 12 ng of each component reached the mass spectrometer. These results essentially confirmed that the LC peak shapes were of sufficient quality, and that the detection limits were below the ng level. Figure 47 illustrates the quality of the full-scan mass spectra obtainable in an LC-MS analysis, for 10 ng of each adduct delivered to the mass spectrometer.

Results of a more serious attempt to determine instrumental detection limits, for ionspray mass spectrometric analysis of these adducts, are summarised in Figure 48. Flow injection analyses of a mixture of purified dG^{AAF} and pdG^{AAF}, using selected ion monitoring, were run with duplicate injections. The mass spectrometric detection limit for each of these adducts is thus estimated to be about 50 pg.

Finally, the ability of the present LC-MS methodology to detect chemically modified nucleosides and nucleotides, in the presence of a large excess of unmodified residues, was

investigated. A solution containing 250 μg/mL of each of pdG and dG, together with 250 ng/mL of each of pdG^{AAF} and dG^{AAF}, was analysed by LC-MS. The results are shown in Figure 49. Since the injection volume was 5 μL and the post-column split ratio was 1:20, only 0.25μL of the test solution reached the mass spectrometer, *i.e.* 60 ng of each of dG and pdG and 60 pg of each of dG^{AAF} and pdG^{AAF} . The detection limits for the adducts (about 30-50 pg) estimated from these LC-MS experiments are similar to those estimated from flow-injection experiments (Figure 48). Thus, the 10^3 -fold excess of unmodified nucleoside and nucleotides did not affect the performance, since the HPLC conditions were such that the excess components did not co-elute with the trace-level adducts. It seems likely that this feature would be valid at even higher excess ratios than that actually attempted.

CONCLUSIONS.

The fraction of modified bases in seriously damaged DNA *in vivo* is of the order of 1 in 10^7 - 10^8. We believe that the present LC-MS methodology could handle the implications of this large molar ratio, with only slight modifications to the HPLC conditions. The limiting feature of this methodology in its present state of development is its absolute sensitivity. If the LC-MS detection limit (using selected ion monitoring) is taken as 50 pg for the adducts of mononucleosides and mononucleotides, a molar ratio of one modified base in 10^7 - 10^8 implies a minimum DNA sample size per LC-MS injection of 1-10 mgs. It is clearly impractical to attempt a direct LC-MS analysis by injection of the entire hydrolysate of such a quantity of DNA. Either the instrumental sensitivity would have to be improved by several orders of magnitude, or some pre-column enrichment procedure, for those DNA fragments modified by hydropholic moieties such as that studied here, would have to be developed. The 4-dimensional TLC procedure developed for the Randerath procedure (*loc. cit.*) could possibly be adapted to this purpose.

If this or some similar clean-up procedure were to be developed, it is possible to envisage an experimental sequence in which 10 mgs of damaged DNA is hydrolysed and those nucleosides or nucleotides which have been modified are greatly enriched so that the enriched fraction can be brought into 10 μL of solution. Use of a 1 mm i.d. HPLC column, with a mobile phase flowrate of 50 μL/min or so, would permit a 1 μL injection volume with 100% transfer to the mass spectrometer (no split), *i.e.* introduction of the modified base content from 1 mg of DNA. The LC-MS detection limit of 50 pg of nucleoside adduct corresponds to about 25 pg of the corresponding unmodified nucleoside, since the molecular weight of a nucleoside adduct is often about double that of the unmodified nucleoside. Thus the detection limit corresponds to 25 pg from 1 mg, a ratio of 1 modified base in $4x10^7$ in the original DNA, which is the correct order of magnitude for DNA damaged by chemical carcinogens and mutagens.

This conclusion is extremely encouraging, since it suggests that the radioactive adducts detected in the Randerath procedure might be susceptible to characterisation by LC-MS. However, some words of caution are in order. The order-of-magnitude calculation outlined in the preceding paragraph implicitly assumed that the hydrolysis and clean-up procedures resulted in no losses of the adducts which are the target analytes. Moreover, the LC-MS detection limit used in the calculation was that determined in the present work for *selected ion monitoring* of a single adduct. In turn, use of this detection limit in the calculation implies that the damaged DNA contains modified bases of only one kind, whose molecular weight is known. Since the proposed procedure involves injection of only 1 μL out of a total of 10 μL of extract, it is possible to make several alternative guesses of the molecular weight if the original estimate turns out to be wrong. However, while the present results are indeed extremely encouraging, the sensitivity of the LC-MS technology in its present state of development is not yet adequate for its routine application to analysis of DNA damaged *in vivo* by chemical carcinogens. For example, if full-scan mass spectra are required to characterise unknown adducts, the sensitivity will have to be improved by up to two orders of magnitude relative to that determined here for selected ion monitoring with just 4 mass channels.

CAPTIONS FOR FIGURES

Figure 1. Structures of characteristic adducts of benzo[a]pyrene metabolite with DNA fragments.

(a) nucleoside (3',5'-diphosphate);
(b) nucleotide (3'-monophosphate);
(c) nucleoside;
(d) DNA base.

Figure 2. Schematic representation of essential features of analytical chromatography.

Figure 3. Schematic representation of essential features of analytical mass spectrometry.

Figure 4. Ionization techniques for mass spectrometry of pre-volatilised compounds.

Figure 5. Some important considerations for gas chromatography with mass spectrometry (GC-MS).

Figure 6. Some considerations for analytical high-performance liquid chromatography (HPLC).

Figure 7. Justification for on-line HPLC with mass spectrometry.

Figure 8. Fundamental problems in LC-MS interfacing.

Figure 9. Current methods for LC-MS interfacing.

Figure 10. Schematic diagram of the moving-belt LC-MS interface.

Figure 11. Schematic diagram of the continuous-flow fast atom bombardment (CF-FAB) interface for LC-MS.

Figure 12. Schematic representation of the thermospray interface for LC-MS.

Figure 13. Schematic representation of the ionspray interface for LC-MS.

Figure 14. Compromises recommended for ionspray LC-MS operation with LC columns of different diameters, and thus different mobile phase flownates.

Figure 15. Typical results obtained by ionspray LC-MS analysis of mussel tissue contaminated by domoic acid.

(a) Reconstructed ion chromatogram for m/z 312, which corresponds to the protonated molecule $(M + H)^+$ of domoic acid.
(b) Mass spectrum acquired at the crest of peak 6 in (a).
(c) Tandem mass spectrum of fragment ions of m/z 312, acquired at the crest of peak 6 in (a)

Figure 16. Schematic representation of principles of tandem mass spectrometry using a triple quadrupole instrument.

Figure 17. Calibration curves for quantitation of the cardiac drug diltiazem (DTZ), and one of its metabolites, using ionspray LC-MS by monitoring the respective protonated molecules $(M + H)^+$.

Figure 18. Diagram showing the mechanism of electroendosmosis, indicating the negative charge on the fused silica capillary wall, the positively charged double layer adjacent to the wall, the electroendosmotic velocity V_{eo}, and the electrophoretic velocity V_{ep}. At high pH the negatively charged analyte species undergo electrophoretic migration towards the positive electrode, but at sufficiently low pH they acquire a positive charge and the electrophoretic velocity is directed towards the negative electrode. The direction of the electroendosmotic flow is always toward the negative electrode, for untreated silica capillaries, but the net concentration of positive charge in the double layer, and thus V_{eo}, varies with pH.

Figure 19. Comparison of the flow profiles characteristic of capillary electroendosmotic flow and of the hydrodynamic flow typical of pressure-induced HPLC flows.

Figure 20. Electropherograms of marine toxin standards in Trisma buffer.
(a) CE/UV analysis (200) of a mixture of STX and TTX standards, approximately 1.5 ng each on-column.
(b) CE/MS analysis of the same solution as that analyzed in (a), approximately 7.4 ng each on-column. Scan range m/z 130-500. Reconstructed ion electropherograms for the most intense ions observed. Note that the migration times are not directly related to those in Figure 20 (a) due to the longer capillary length required for CE-MS coupling.

Figure 21.
(a) UV absorption spectrum of guanine (a).
(b) MS-MS spectrum of the $(M + H)^+$ ion of G, obtained by ionspray ionisation of an acidified solution of G, with flow injection.

Figure 22.

(a) Positive-ion ionspray mass spectrum of N2-acetylguanine; flow injection.
(b) Fragment ion spectrum of protonated N2-acetylguanine, obtained by MS-MS of $(M + H)^+$ ion at m/z 194.

Figure 23. Spectroscopic data for 2'-deoxyguanosine (dG).

(a) UV spectrum.
(b) Positive-ion ionspray mass spectrum; flow injection.
(c) Fragment ion spectrum of protonated dG, obtained by MS-MS of $(M + H)^+$ ion at m/z 268.
(d) Fragment ion spectrum of ion observed at m/z 152 in the mass spectrum of dG (Figure 23 (b)).

Figure 24. Positive-ion ionspray mass spectrum of guanosine (rG), (i.e. non-reduced ribose); flow injection.

Figure 25. Positive-ion ionspray mass spectrum of 2'-deoxyadenosine (dA); flow injection.

Figure 26. Spectra for 2'-deoxyguanosine-5'-monophosphate (pdG) and for 2'-deoxyguanosine-3'-monophosphate (dGp).

(a) UV spectrum.
(b) Positive - ion ionspray mass spectrum; flow injection.
(c) Fragment ion spectrum from MS-MS of protonated pdG (m/z 348).
(d) Fragment-ion spectrum from MS-MS of protonated dGp (m/z 348, isomer of pdG shown in (c)).

Figure 27. Fragment ion spectrum of protonated N2-isobutyryl-2'-deoxyguanosine (N2-isobutyryl-dG); $(M+H)^+$ ion at m/z 338.

Figure 28. Fragment ion spectrum of protonated N2-isobutyryl-2'-deoxyguanosine-5'-monophosphate (N2-isobutyryl-pdG); $(M+H)^+$ ion at m/z 418.

Figure 29. Positive-ion ionspray mass spectrum of the dinucleoside monophosphate 2'-deoxyadenosine-(3'-5')-2'-deoxycytidine (dApdC); flow injection.

Figure 30. Positive-ion ionspray mass spectrum of the dinucleoside monophosphate, 2'-deoxyadenosine-(3'-5')-2'-deoxyguanosine (dApdG); flow injection.

Figure 31. Reaction scheme for N-acetoxy-2-N-acetylaminofluorene (NA-AAF) with 2'-deoxyguanosine (dG) and with 2'-deoxyguanosine-5'-monophosphate (pdG).

Figure 32. LC-MS analysis of reaction products resulting from reaction of NA-AAF with pdG. HPLC conditions: isocratic mobile phase, 60% methanol with 0.1% trifluoroacetic acid, 1mL/min flowrate, 4.6 mm i.d. Zorbax Rx-C8 column. HPLC effluent was split in a 1:20 ratio, delivering 50 μL/min to the ionspray interface of the SCIEX API III mass spectrometer. Injection volume 20μL. Selected ion monitoring was used to obtain the following mass chromatograms:

(a) m/z 331; $(M + H)^+$ ion for G^{AF} .
(b) m/z 348; $(M + H)^+$ ion for pdG (and for dGp).
(c) m/z 373; $(M + H)^+$ ion for pdG^{AAF}.
(d) m/z 569; $(M + H)^+$ ion for G^{AAF} .

Figure 33. LC-MS analysis of reaction products resulting from reaction of NA-AAF with dG. HPLC conditions same as for Figure 32. Selected ion monitoring was used to obtain the following mass chromatograms:

(a) m/z 268; $(M + H)^+$ ion for dG.
(b) m/z 331; $(M + H)^+$ ion for G^{AF}.
(c) m/z 373; $(M + H)^+$ ion for G^{AAF}.
(d) m/z 489; $(M + H)^+$ ion for dG^{AAF} .

Figure 34. LC-MS analysis of reaction products resulting from hydrolysis of dG^{AAF} by dilute HCL. HPLC conditions same as for Figure 32. Selected ion monitoring was used to obtain the following mass chromatograms:

(a) m/z 152; $(M + H)^+$ ion for G.
(b) m/z 331; $(M + H)^+$ ion for G^{AF}.
(c) m/z 373; $(M + H)^+$ ion for G^{AAF}.
(d) m/z 489; $(M + H)^+$ ion for dG^{AAF} .

Figure 35. LC-MS analysis of reaction products resulting from hydrolysis of dG^{AAF} with concentrated HCL. HPLC conditions same as for Figure 32. Selected ion monitoring was used to obtain the following mass chromatograms:

(a) m/z 152; $(M + H)^+$ ion for G.
(b) m/z 331; $(M + H)^+$ ion for G^{AF}.
(c) m/z 373; $(M + H)^+$ ion for G^{AAF}.
(d) m/z 489; $(M + H)^+$ ion for dG^{AAF} .

Figure 36. LC-MS analysis of reaction products resulting from hydrolysis of pdG^{AAF} with NaOH. HPLC conditions same as for Figure 32. Selected ion monitoring was used to obtain the following mass chromatograms:

(a) m/z 348; $(M + H)^+$ ion for pdG.
(b) m/z 431; $Na_4(TFAc)_3^+$ cluster ion eluting at t_o.
(c) m/z 527; $(M + H)^+$ ion for pdG^{AF}.
(d) m/z 543; $(M + H)^+$ ion for pdG^{AFOH} .
(e) m/z 567; Na_5 $(TFAc)^+$ cluster ion at t_o; (TFAc denotes CF_3 CO_2^- anion).

Figure 37. LC-MS analysis of reaction products resulting from hydrolysis of dG^{AAF} with NaOH. HPLC conditions same as for Figure 32. Selected ion monitoring was used to obtain the following mass chromatograms:

(a) m/z 347; $(M + H)^+$ ion for G^{AFOH}.
(b) m/z 431; $Na_4(TFAc)_3^+$ cluster ion eluting at t_o.
(c) m/z 447; unidentified salt cluster ion eluting at t_o.
(d) m/z 463; $(M + H)^+$ ion for dG^{AFOH} .
(e) m/z 567; Na_5 $(TFAc)^+$ cluster ion at t_o (TFAc denotes CF_3 CO_2^-).

Figure 38. LC-MS analysis of same reaction mixture as in Figure 36 (NaOH hydrolysis of pdG^{AAF}) but with improved HPLC conditions (isocratic, 40% methanol, 0.1% trifluoroacetic acid). Selected ion monitoring was used to obtain the following mass chromatograms:

(a) m/z 347; $(M + H)^+$ ion for G^{AFOH}.
(b) m/z 463; $(M + H)^+$ ion for dG^{AFOH}.
(c) m/z 543; $(M + H)^+$ ion for pdG^{AFOH}.
(d) m/z 567; Na_5 $(TFAc)^+$ cluster ion at t_o (TFAc denotes CF_3 CO_2^-).

Figure 39. LC-MS analysis of same reaction mixture as in Figure 37 (NaOH hydrolysis of dG^{AAF})but with improved HPLC conditions (isocratic, 40% methanol, 0.1% trifluoroacetic acid). Selected ion monitoring was used to obtain the following mass chromatograms:

(a) m/z 347; $(M + H)^+$ ion for G^{AFOH}.
(b) m/z 463; $(M + H)^+$ ion for dG^{AFOH}.
(c) m/z 543; $(M + H)^+$ ion for pdG^{AFOH}.
(d) m/z 567; Na_5 $(TFAc)^+$ cluster ion at t_o (TFAc denotes CF_3 CO_2^-).

Figure 40. Spectroscopic data for dG^{AAF} adduct. All spectra were acquired by on-line LC-UV or LC-MS experiments.

(a) UV-visible spectrum
(b) Positive ion ionspray mass spectrum.
(c) Fragment ion spectrum obtained by MS-MS experiment on $(M + H)^+$ ion of dG^{AAF} (m/z 489, Figure 40b).
(d) Fragment ion spectrum obtained by MS-MS experiment on ion at m/z 373 observed in ionspray mass spectrum of dG^{AAF} (Figure 40b).

Figure 41. Spectroscopic data for pdG^{AAF} adduct. All spectra were acquired by on-line LC-UV or LC-MS experiments.

(a) UV-visible spectrum
(b) Positive ion ionspray mass spectrum.
(c) Fragment ion spectrum obtained by MS-MS experiment on $(M + H)^+$ ion of pdG^{AAF} (m/z 569, Figure 41b).
(d) Fragment ion spectrum obtained by MS-MS experiment on ion at m/z 373 observed in ionspray mass spectrum of pdG^{AAF} (Figure 41b).

Figure 42. Spectroscopic data for G^{AAF} adduct. Both spectra were acquired by on-line LC-UV or LC-MS experiments.

(a) UV-visible spectrum
(b) Positive ion ionspray mass spectrum.

Figure 43. Spectroscopic data for G^{AF} adduct. All spectra were acquired by on-line LC-UV or LC-MS experiments.

(a) UV-visible spectrum
(b) Positive ion ionspray mass spectrum.

Figure 44. Spectroscopic data for G^{AFOH} adduct. Both spectra were acquired by on-line LC-UV or LC-MS experiments.

(a) UV-visible spectrum
(b) Positive ion ionspray mass spectrum.

Figure 45. Spectroscopic data for pdG^{AFOH} adduct. All spectra were acquired by on-line LC-UV or LC-MS experiments.

(a) UV-visible spectrum
(b) Positive ion ionspray mass spectrum.

Figure 46. LC-MS analysis of a mixture of 2'-deoxyguanosine and 2'-deoxyguanosine-5'-monophosphate, their NA-AAF adducts, and the hydrolysis products thereof. Concentrations of the adducts were all approximately 50μg/mL. HPLC conditions the same as for Figure 32. Post-column split 1:20 (mass spectrometer : waste), 5 μL injection on column. Selected ion monitoring was used to obtain the mass chromatograms. The shaded LC peaks are those indentified (via retention times) as due to the $(M+H)^+$ ions of the target analytes indicated (other non-shaded peaks are due to fragment ions from $(M+H)^+$ ions of other components of the mixture):

(a) m/z 268; $(M + H)^+$ ion of dG.
(b) m/z 331; $(M + H)^+$ ion of G^{AF}.
(c) m/z 348; $(M + H)^+$ ion of pdG.
(d) m/z 373; $(M + H)^+$ ion of G^{AAF}.
(e) m/z 489; $(M + H)^+$ ion of dG^{AAF}.
(f) m/z 569; $(M + H)^+$ ion of pdG^{AAF}.

Figure 47. Full-scan mass spectra obtained by LC-MS analysis of a mixture of dG^{AAF} and pdG^{AAF}. HPLC conditions a 1 mm i.d. column, the same mobile phase as in Figure 32 at a flowrate of 50 μL/min, a 1 μL injection volume, and no post-column split. Amounts injected on-column were 10ng of each adduct.

(a) Spectrum acquired at correct retention time for dG^{AAF}
(b) Spectrum acquired at correct retention time for pdG^{AAF}

Figure 48. Flow-injection mass spectrometric analysis, using selected ion monitoring, of a mixture of purified adducts dG^{AAF} and pdG^{AAF}. Amounts injected are indicated. Ions monitored include the $(M+H)^+$ ions of each adduct (m/z 489 and 569 for dG^{AAF} and pdG^{AAF}, respectively) and m/z 373 which corresponds to protonated G^{AAF} formed as a fragment ion of each of the two adducts injected. The bottom three traces are identical to the top three, but expanded by a factor of 32.

Figure 49. LC-MS analysis of a mixture of pdG (250 μg/mL) plus the adducts pdG^{AAF} and dG^{AAF} (each 250 ng/mL). HPLC conditions same as for Figure 32; post-column split of 1:20 (mass spectrometer : waste), 5μL injected on-column. Selected ion monitoring was used to obtain the following mass chromatograms.

(a) m/z 348; $(M+H)^+$ ion from pdG
(b) m/z 373; protonated G^{AAF}, formed as fragment ion from $(M+H)^+$ ions of dG^{AAF} and of pdG^{AAF}
(c) m/z 489; $(M+H)^+$ ion from dG^{AAF}
(d) m/z 569; $(M+H)^+$ ions from pdG^{AAF}.

Figure 1.

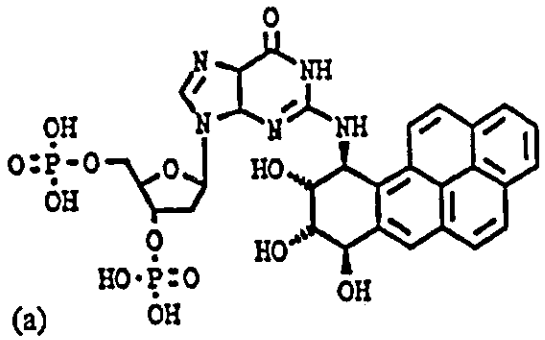

(a)

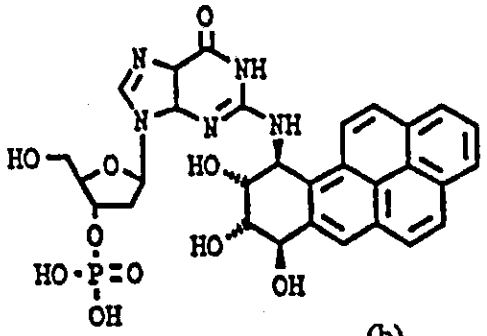

(b)

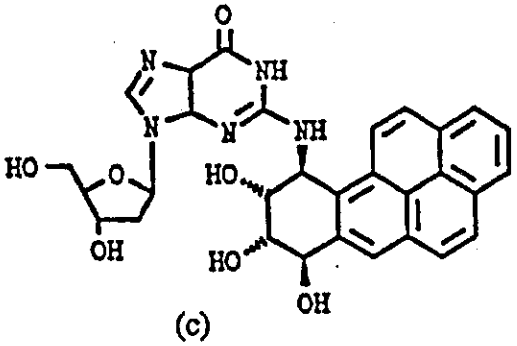

(c)

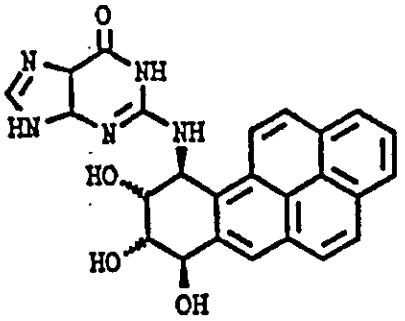

(d)

Figure 2.

Analytical Chromatography

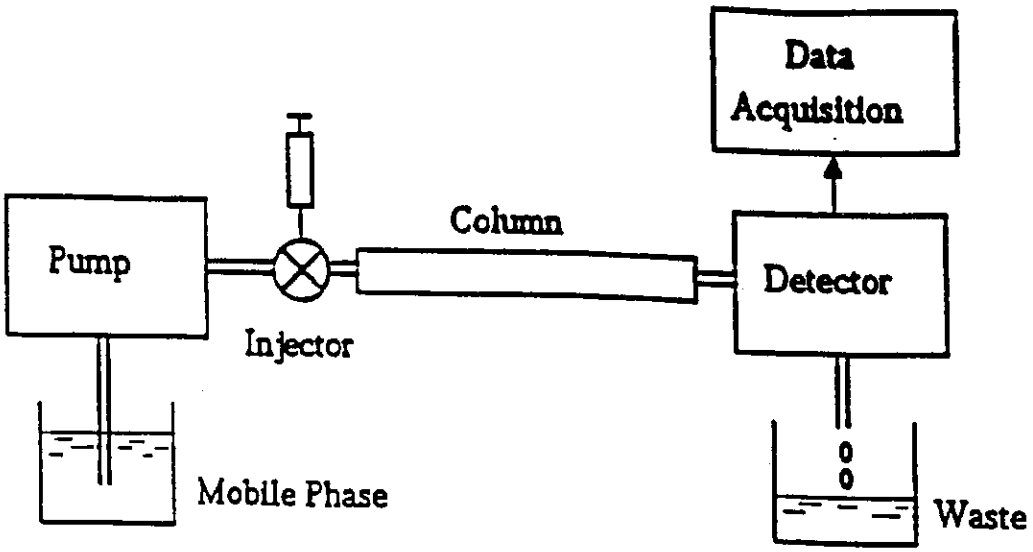

Importance:

* Separation of complex mixtures
* Separation of isomers
* Routine quantitative analysis
* Confirmation of compound identity
  (retention time and selective detectors)

Types:

* Gas chromatography (GC)
* Liquid chromatography (LC, HPLC)
* Supercritical fluid chromatography (SFC)
* Capillary electrophoresis (CE, HPCE, CZE)

Figure 3.

Mass Spectrometry

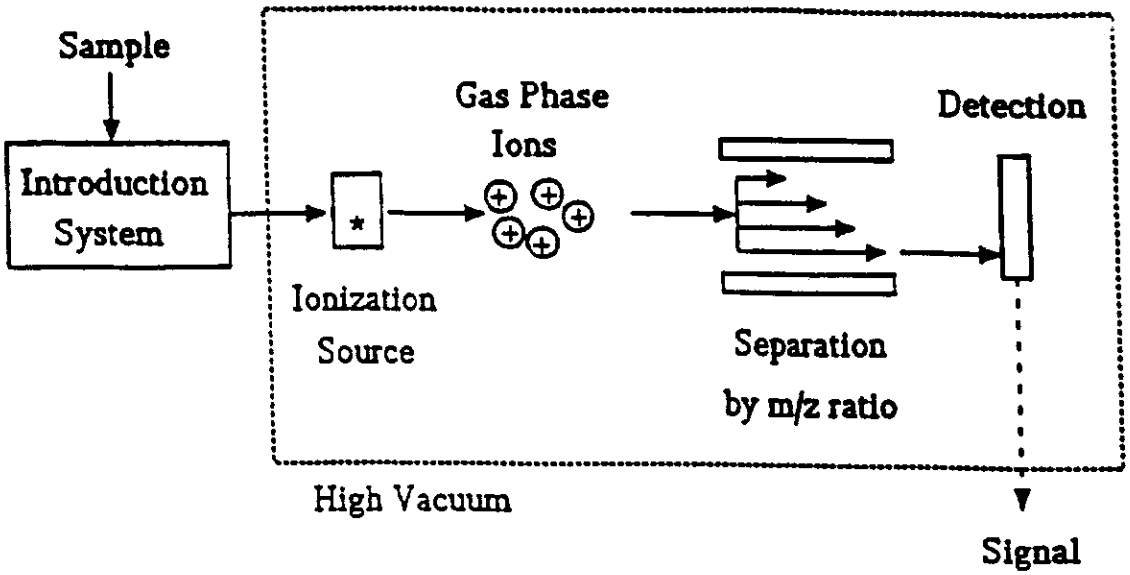

Importance:

* Molecular weight
* Elemental composition
* Structure information (fragmentation, MS/MS)
* High sensitivity
* Universal detection
* Selective detection

Figure 4.

Electron Ionization

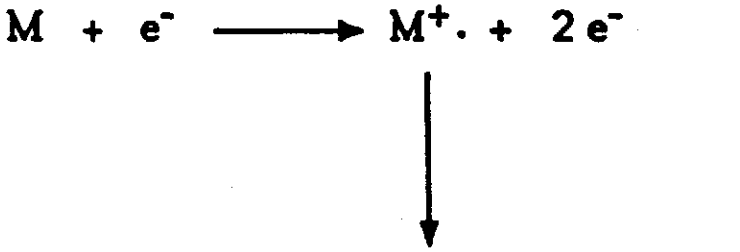

Fragment Ions and Neutrals

Chemical Ionization

Figure 5.

Gas Chromatography - Mass Spectrometry (GC-MS)

Interfaces:

* Effusion separator
* Membrane separator
* Jet separator
* Direct connection of capillary columns

Advantages:

* Mature, easy-to-use technique
* High resolution separations
* Very sensitive (100 pg full scan)
* Numerous detectors for GC prior to GC-MS

Limitations:

* Not suitable for high MW compounds
* Not suitable for thermally labile/low volatility compounds
  (derivatization may be used to enhance volatility)
* Poor injection volume precision
  (internal standards required for quantitation)

Figure 6.

Liquid Chromatography (LC, HPLC)

Advantages:

* Adjustable separation selectivity
  (mobile and stationary phases, column temp)
* Suitable for high MW compounds
* Suitable for thermally labile compounds
* Excellent for quantitative analysis
* Preparative capabilities (NMR, bioassay, LSC, etc.)
* On-line acquisition of optical spectra
* Several sensitive and selective detectors
  (UV, fluorescence, electrochemical, etc.)

Limitations:

* Lower column efficiency than GC
* Lacks a universal sensitive detector

Figure 7.

Combined LC-MS ?

Why not off-line?

* LC has good preparative capabilities
* Independent optimization and scheduling of instruments
* Choice of ionization methods

Why on-line LC-MS?

* Universal yet selective and sensitive detection
* Complex mixture analysis
* Quantitative analysis
* Search for new compounds
* Special ionization methods

Figure 8.

Fundamental Problems in LC-MS Interfacing

1. The mobile phase:
   a) flow rate mismatch problem
      MS pumping speed = 5 mL/min gas max.
      LC at 1 mL/min = 1200 mL/min gas (water)
   b) mobile phase modifiers
      (acids, buffers, ion-pair reagents, etc.)
   c) gradient elution
      (changing mobile phase composition)
2. Wide range of analyte types:
   a) stable to thermally labile
   b) non-polar to polar, including salts
   c) volatile to non-volatile
   d) low MW to high MW
3. Which ionization method to use?
   (EI, CI, FAB, etc.)
4. Chromatographic performance must be maintained

Figure 9.

LC-MS Interfacing Methods

Mobile phase removal	Ionization
* Moving belt interface	EI, CI, FAB
* Particle beam interface (MAGIC)	EI, CI
Flow rate reduction (splitting or micro-LC)	
* Direct liquid injection	CI
* Continuous flow FAB	FAB
Special ionization/interface methods	
* Thermospray	TSP
* Atmospheric pressure ionization	API
- Heated pneumatic nebulizer	APCI
- Electrospray	ESP
- Ion-spray	ISP

Figure 10.

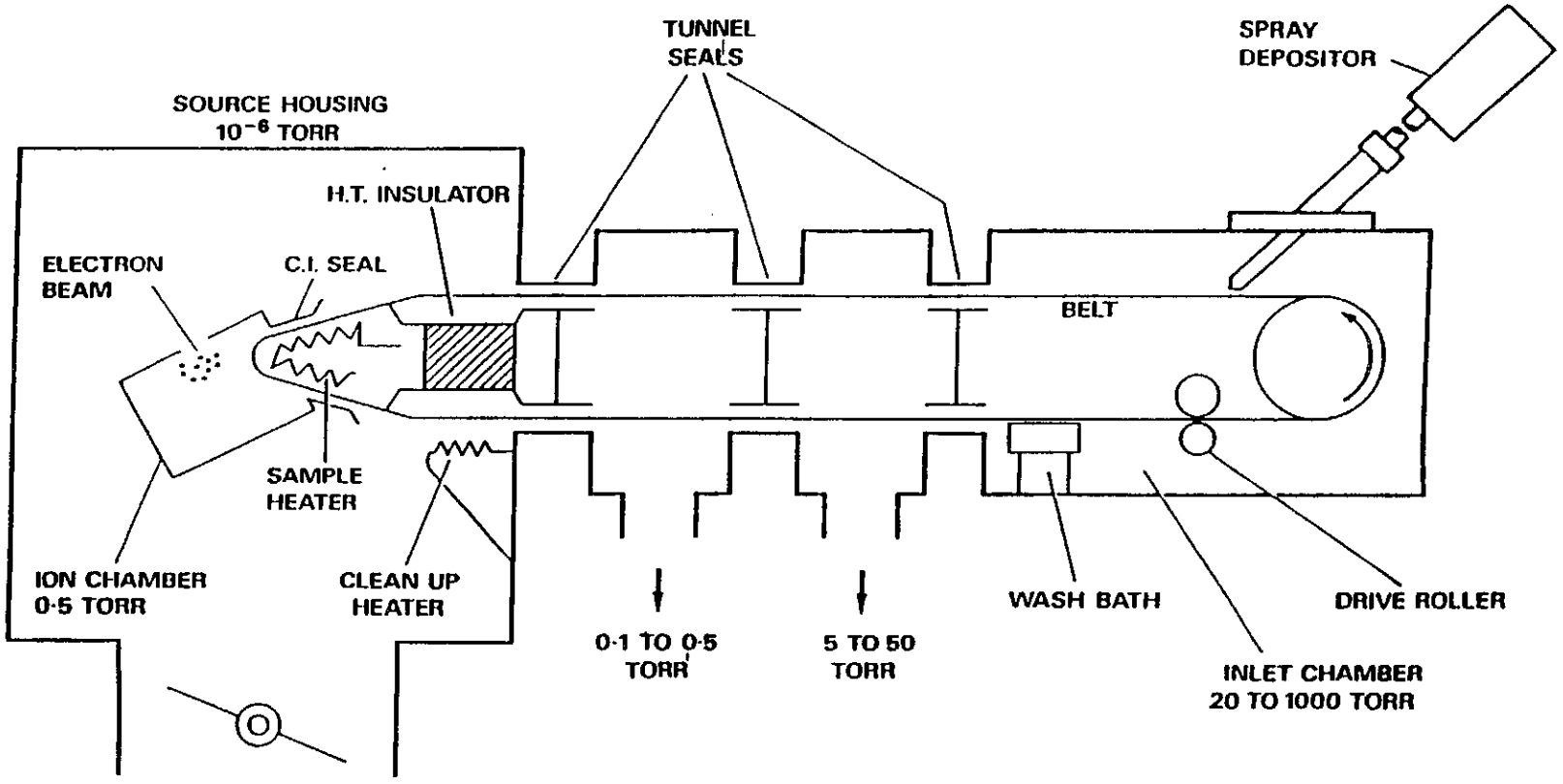
Moving Belt LC-MS Interface
TUNNEL SEALS
SPRAY DEPOSITOR
SOURCE HOUSING 10⁻⁶ TORR
H.T. INSULATOR
ELECTRON BEAM
C.I. SEAL
BELT
SAMPLE HEATER
ION CHAMBER 0·5 TORR
CLEAN UP HEATER
0·1 TO 0·5 TORR
5 TO 50 TORR
WASH BATH
DRIVE ROLLER
INLET CHAMBER 20 TO 1000 TORR

Figure 11.

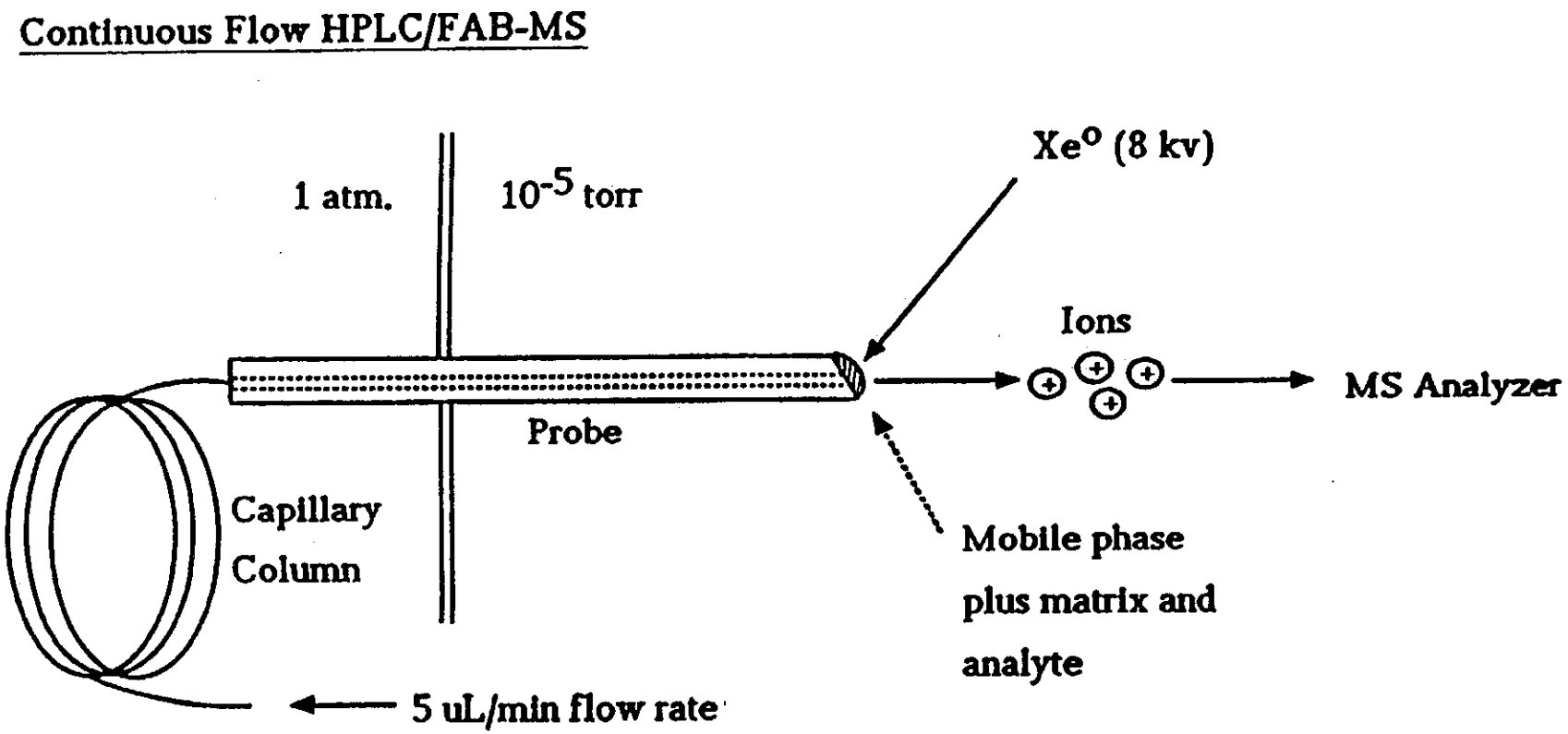
Continuous Flow HPLC/FAB-MS
1 atm.
10-5 torr
Xe° (8 kv)
Ions
MS Analyzer
Probe
Capillary
Column
Mobile phase
plus matrix and
analyte
5 uL/min flow rate

Figure 12.

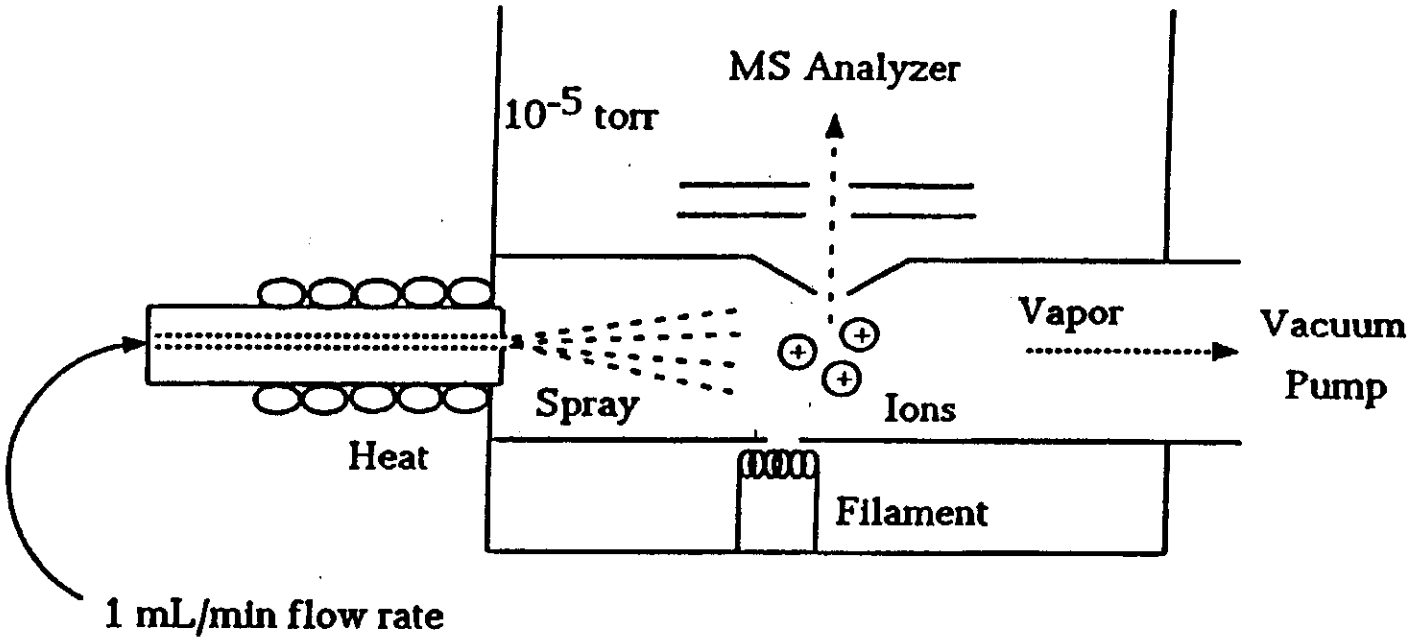

Thermospray LC-MS Interface

Figure 13.

IonSpray Mass Spectrometry

- Atmospheric pressure ionization method.
- Mechanism: "ion evaporation".

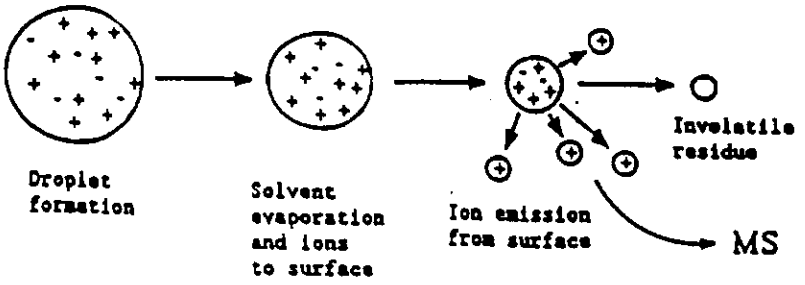

- High sensitivity for polar compounds.
- Flow rates: 1 to 200 uL/min.
- Very easy to interface to HPLC.

A.P. Bruins. T.R. Covey and J.D. Henion,
Anal. Chem. 59, 2642 (1987).

The IonSpray API interface for combined liquid chromatography-mass spectrometry

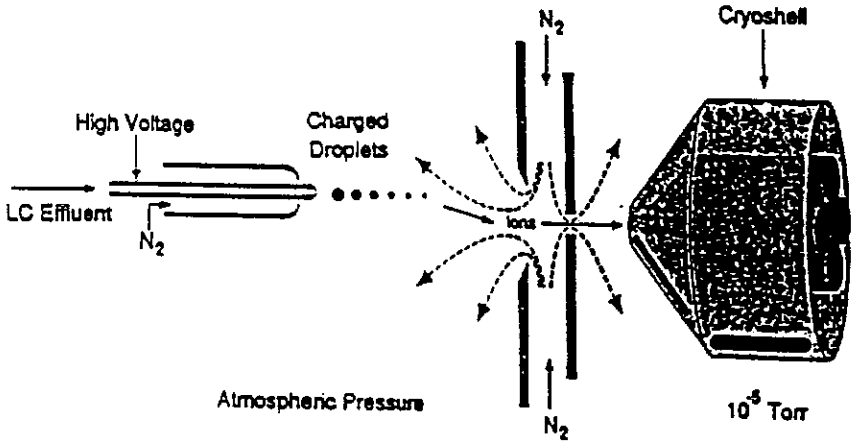

LC Configurations for combined LC-ISP-MS

Figure 14.

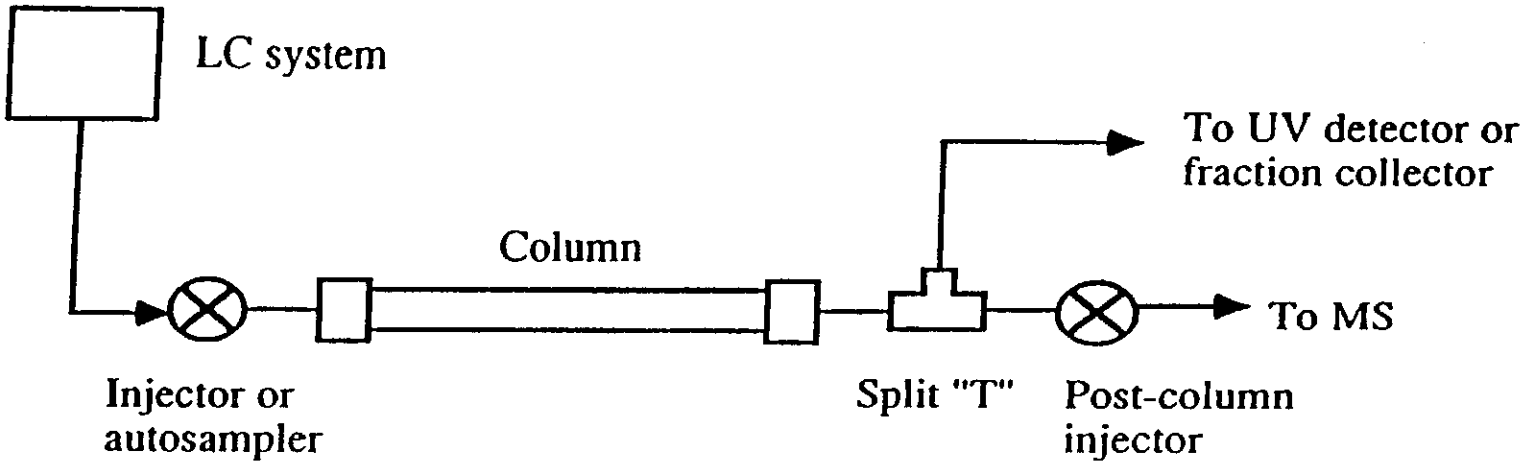

Flow rate (µL/min)	Injection volume (µL)	Column I.D. (mm)	Split	Post column injection vol. (µL)	Mode
1000	25.0	4.6	20	5.0	Semi. Prep Minor peaks
200	5.0	2.1	4 (direct)	1.0	Method dvlp. Analytical (DAD)
50	1.0	1.0	direct	0.1	Analytical
5	0.1	0.32	direct	0.06	Sample limited

Figure 15.

(a) **HPLC/IonSpray-MS**

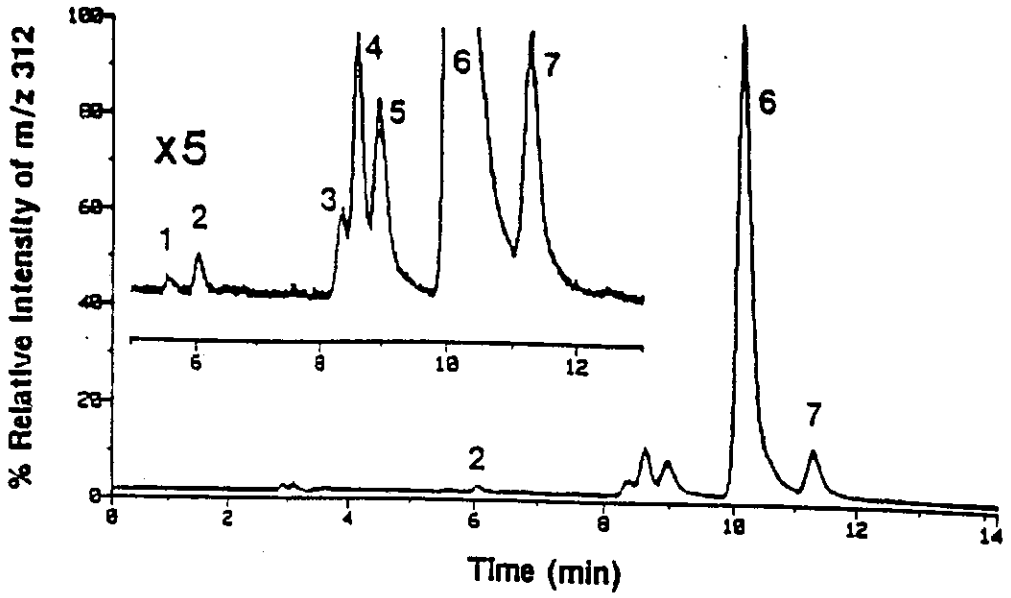

(b) Positive IonSpray Mass Spectrum

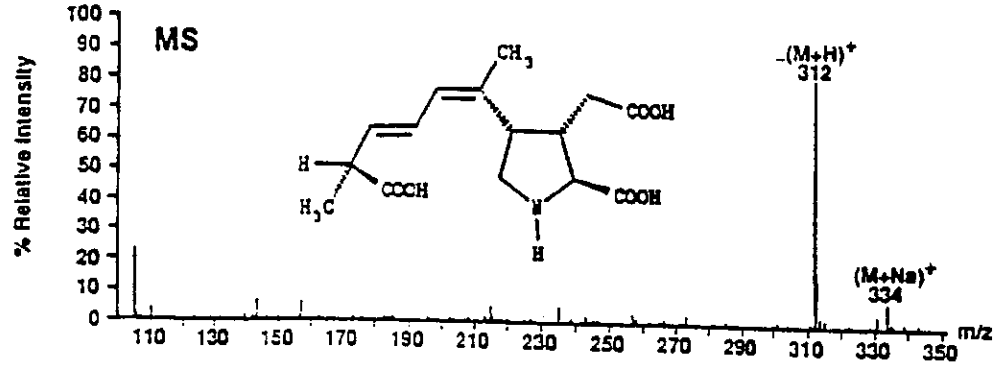

(c)

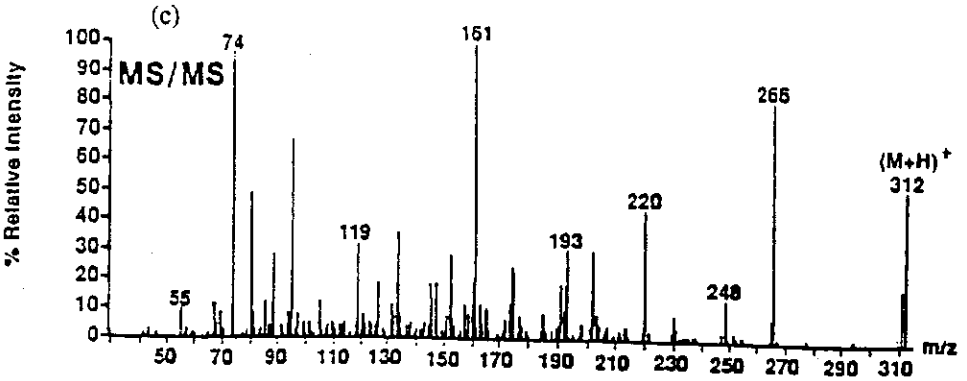

Figure 16.

Tandem Mass Spectrometry with the Triple Quadrupole SCIEX API-III

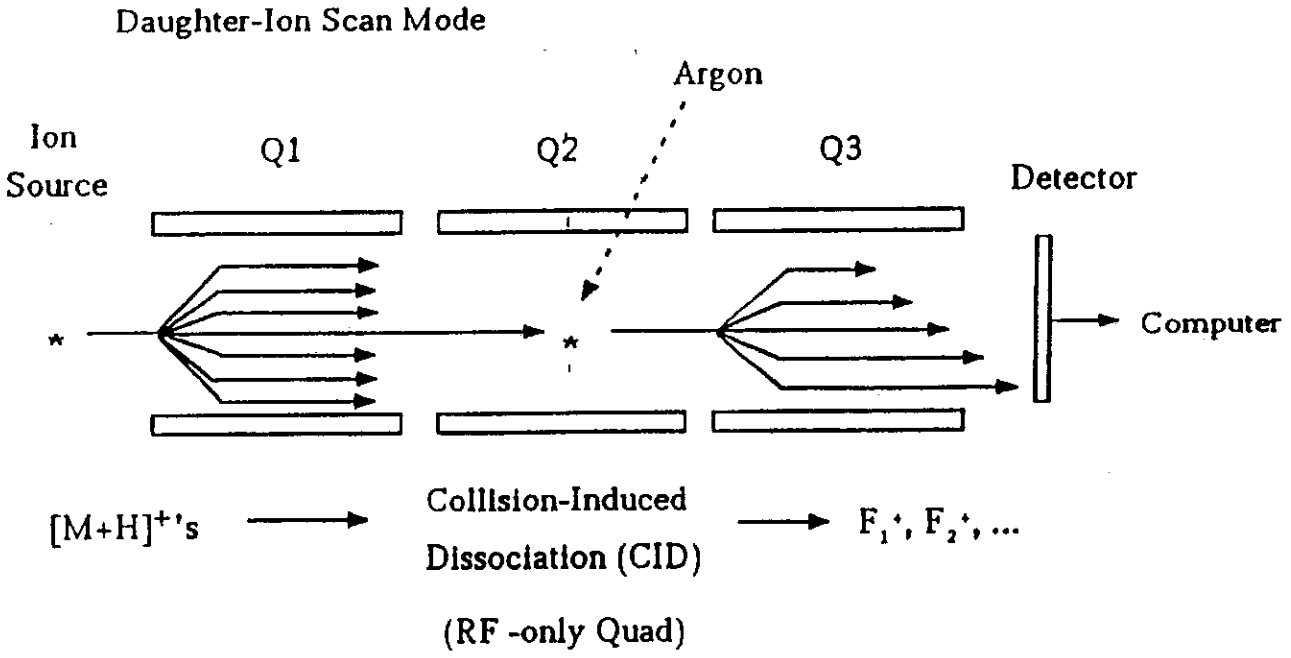

Figure 17.

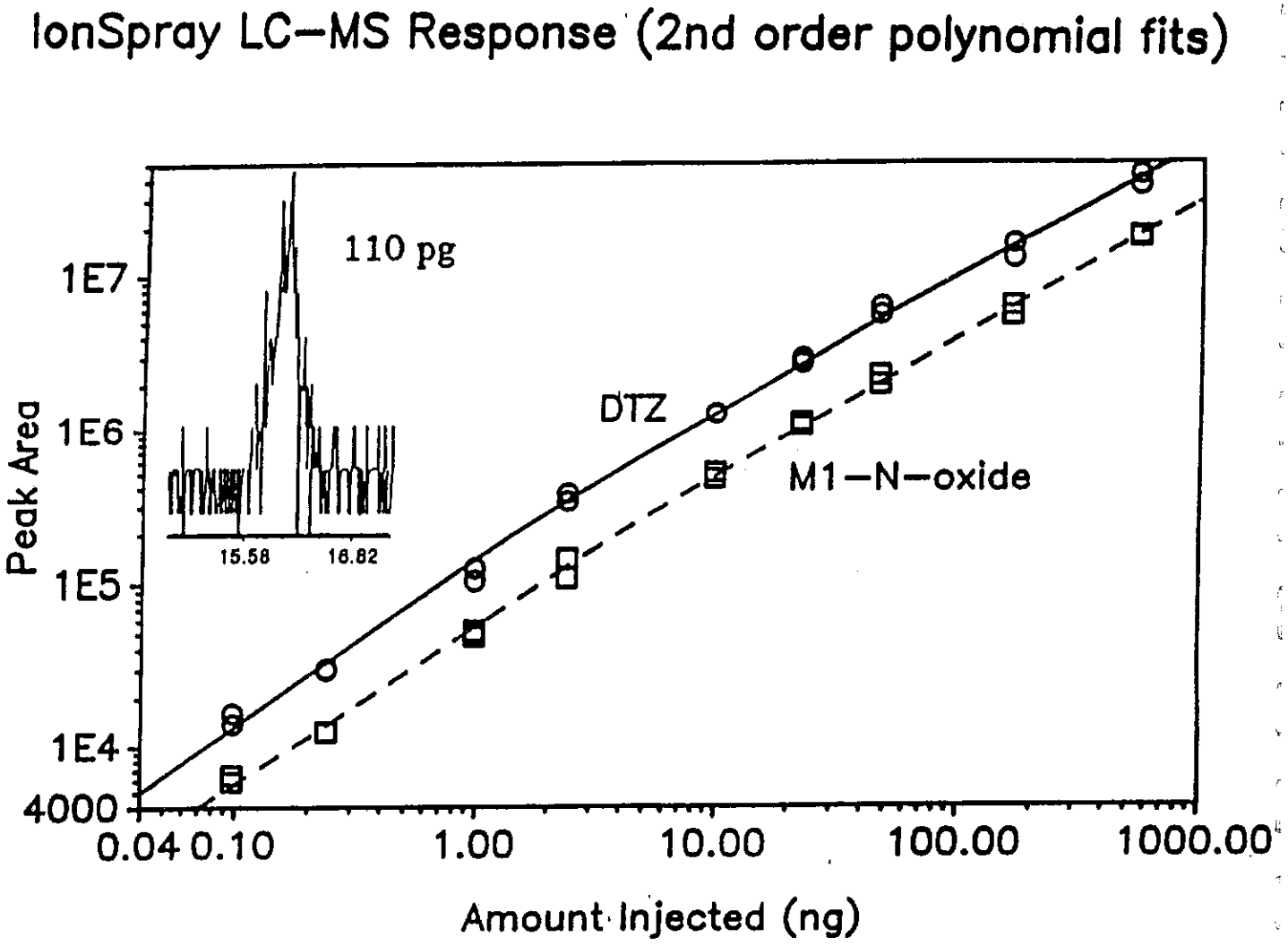
IonSpray LC–MS Response (2nd order polynomial fits)
110 pg
15.58
16.82
DTZ
M1–N–oxide
Peak Area
1E7
1E6
1E5
1E4
4000
0.04
0.10
1.00
10.00
100.00
1000.00
Amount Injected (ng)

Figure 18.

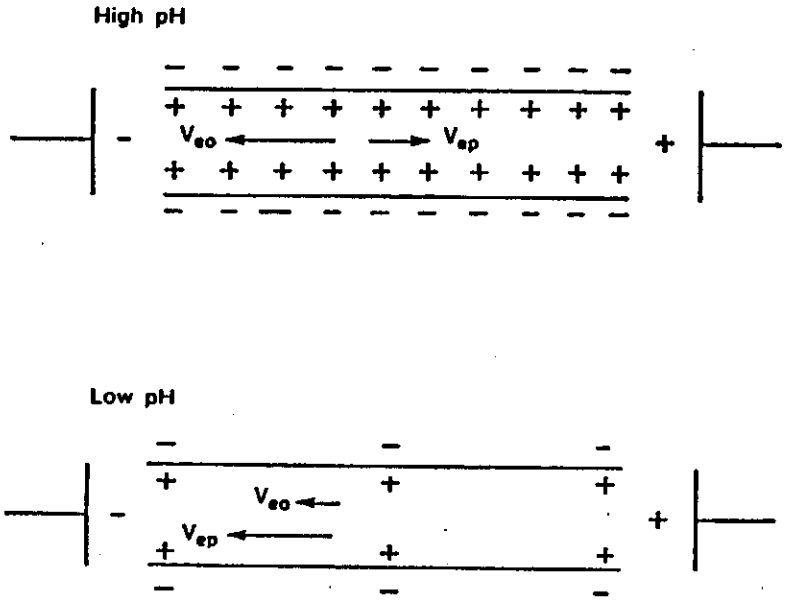

Figure 19.

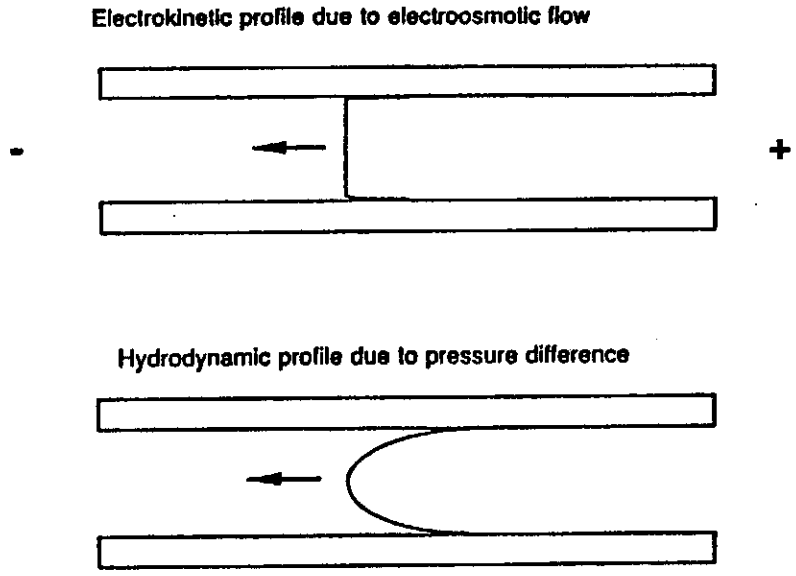
Electrokinetic profile due to electroosmotic flow
-
+
Hydrodynamic profile due to pressure difference

Figure 20.

(a) CE/UV analysis of TTX/STX (150 µg/mL each)
10 nL inj., Trisma pH 7.2, 30 kV

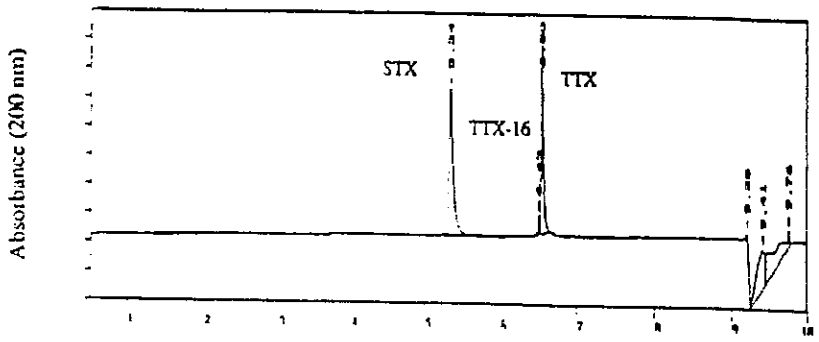

(b) CE/MS analysis of TTX/STX (150 µg/mL each) full scan (130-500 Da)
50 nL inj., Trisma pH 7.2, 24 kV effective

320/320

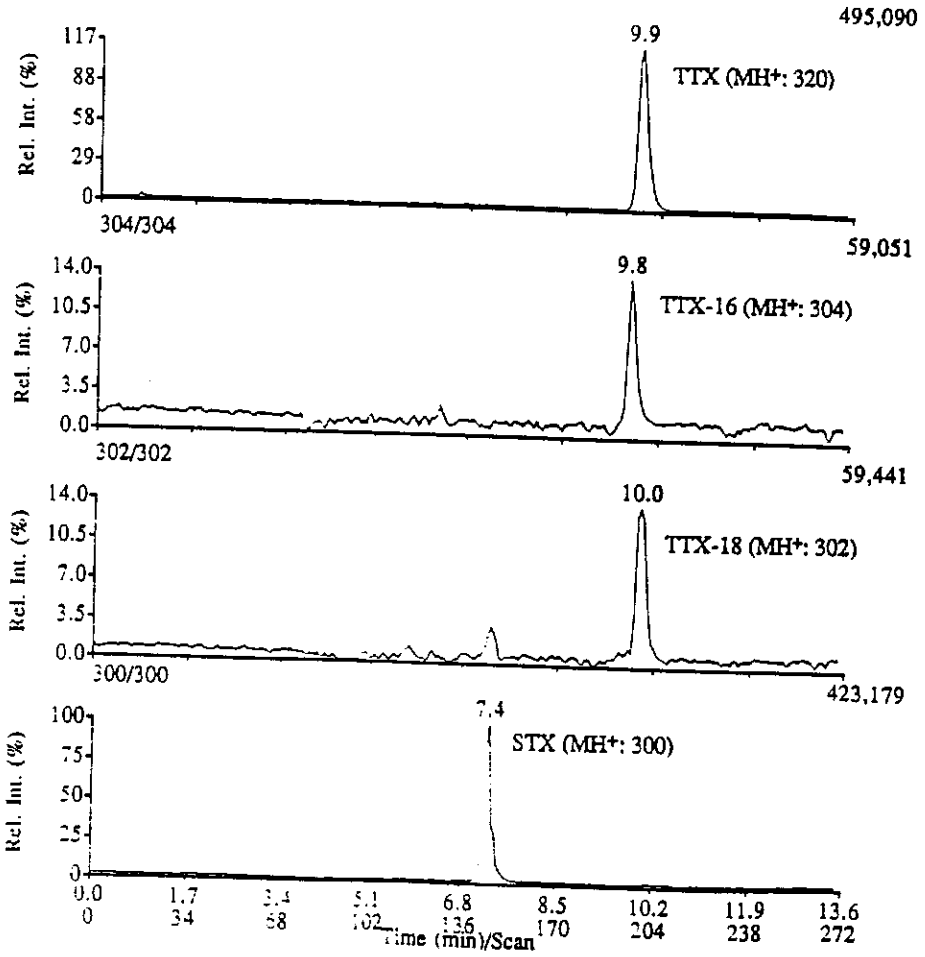

Figure 21.

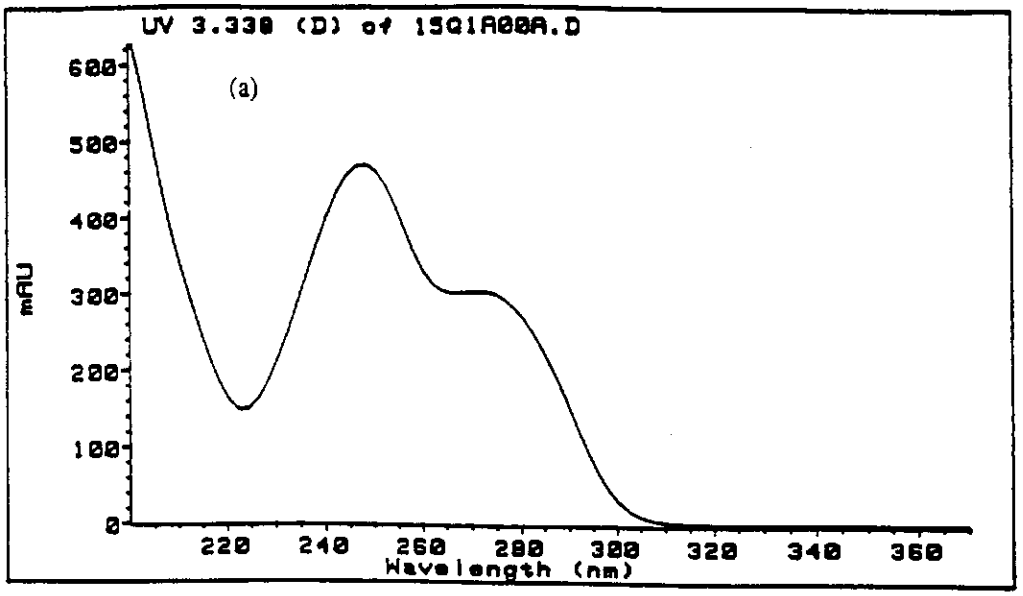
UV 3.338 (D) of 1501A08A.D
(a)
mAU
600
500
400
300
200
100
0
220
240
260
280
300
320
340
360
Wavelength (nm)

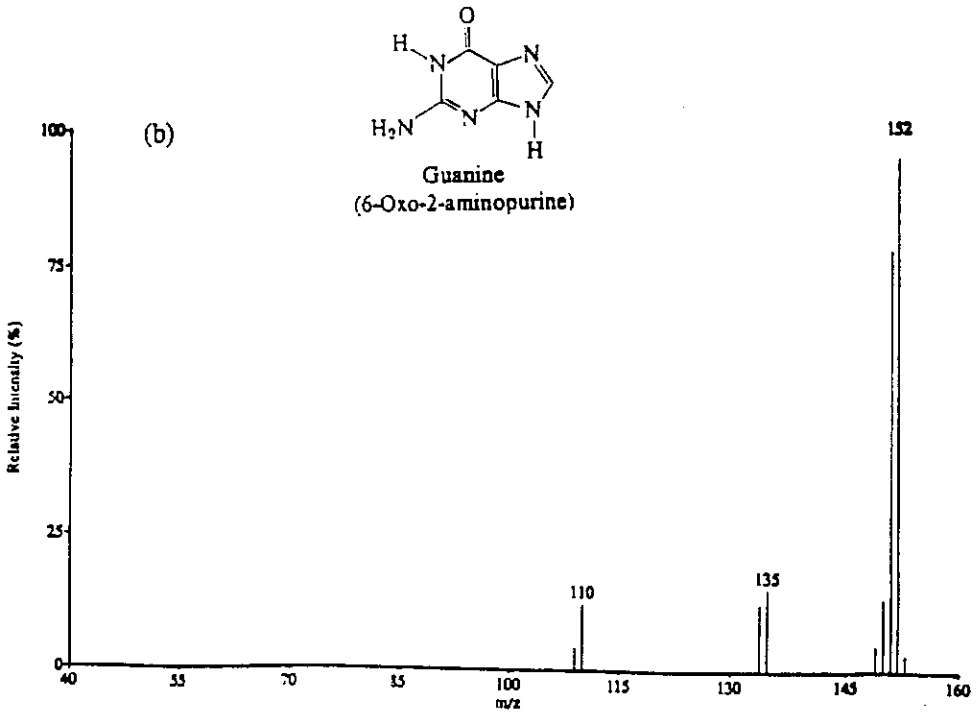
(b)
Guanine
(6-Oxo-2-aminopurine)
Relative Intensity (%)
100
75
50
25
0
110
135
152
40
55
70
85
100
115
130
145
160
m/z

Figure 22.

N2-acetyl guanine

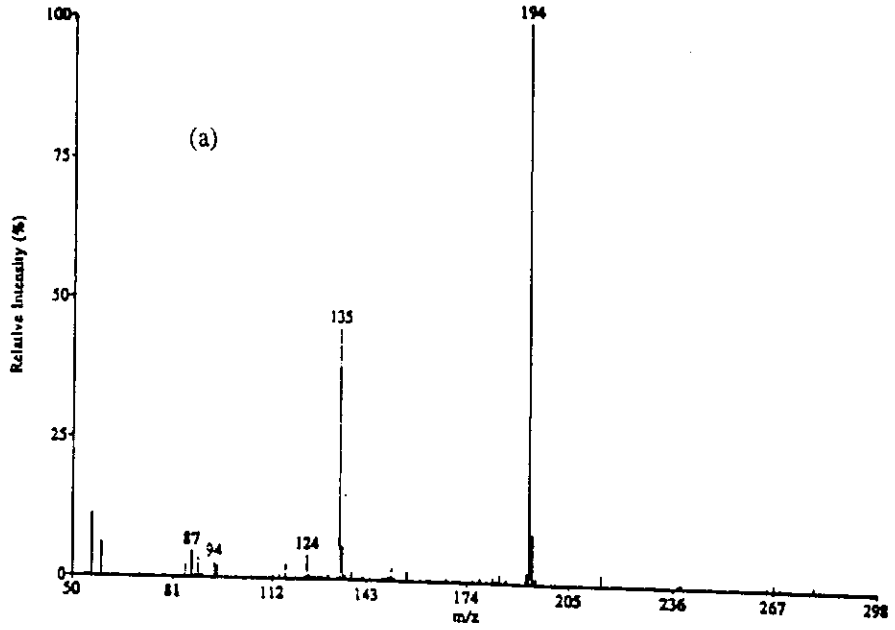

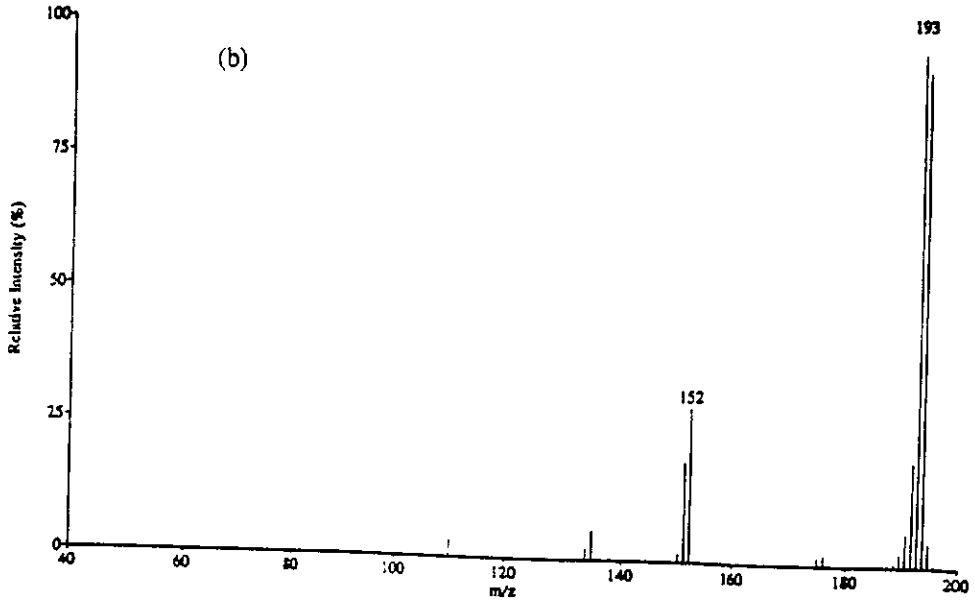

Figure 23.

Spectroscopic data for 2'-deoxyguanosine (dG)

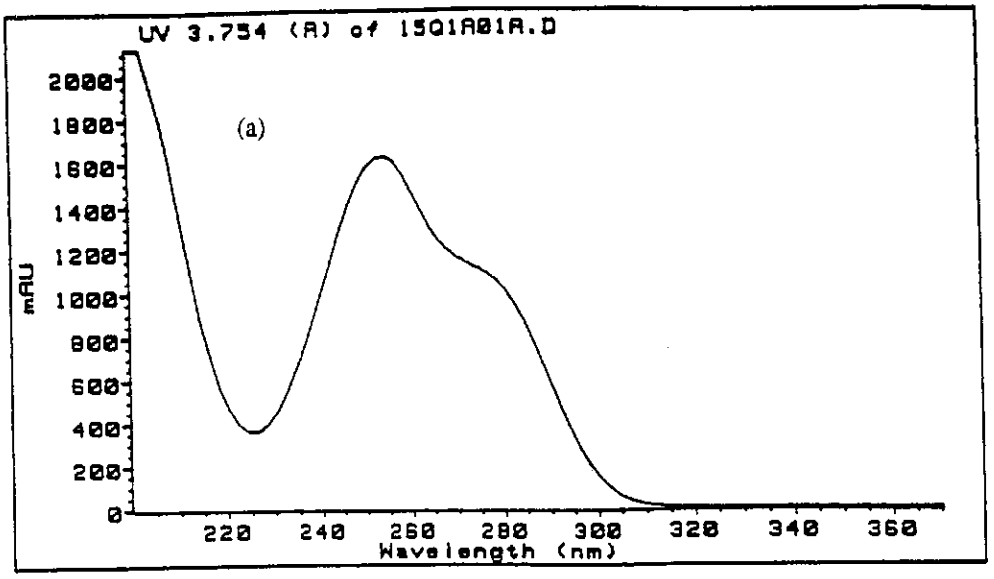

(b)

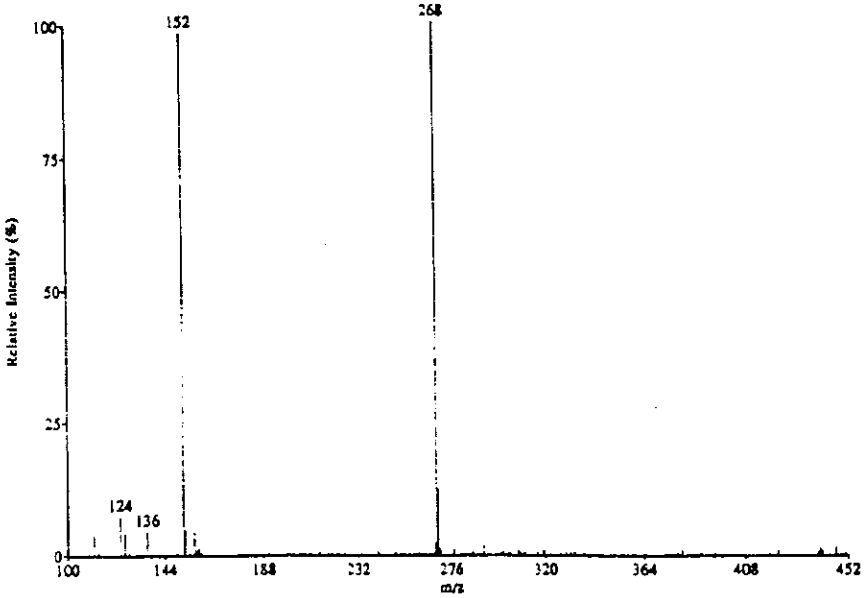

Figure 23.

Spectroscopic data for 2'-deoxyguanosine (dG)

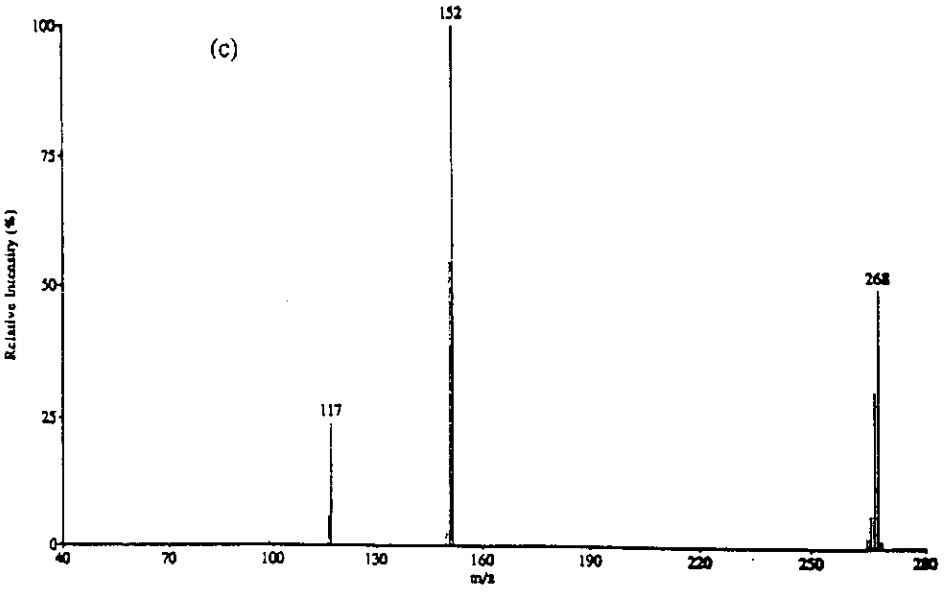

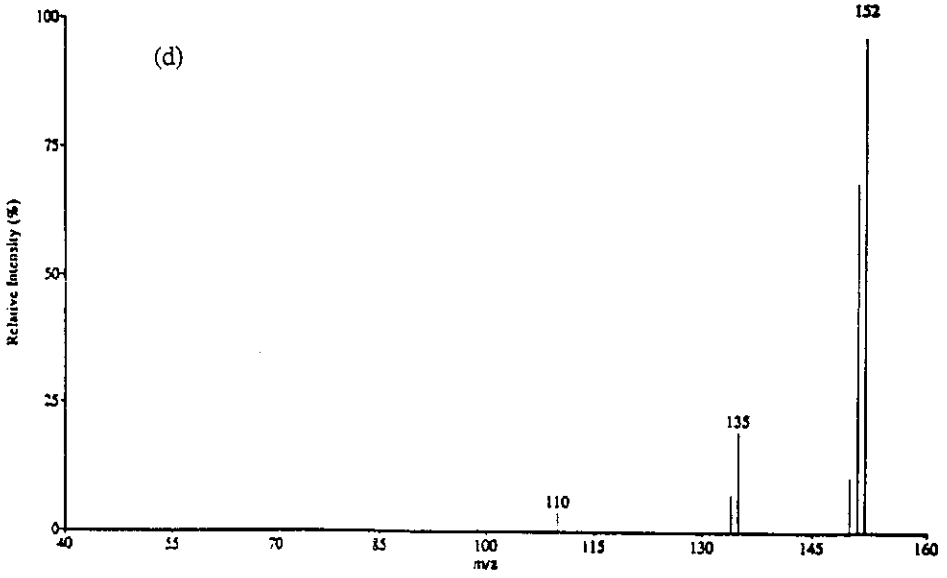

Figure 24.

Positive ion ionspray mass spectrum of guanosine rG, (i.e. non-reduced ribose)

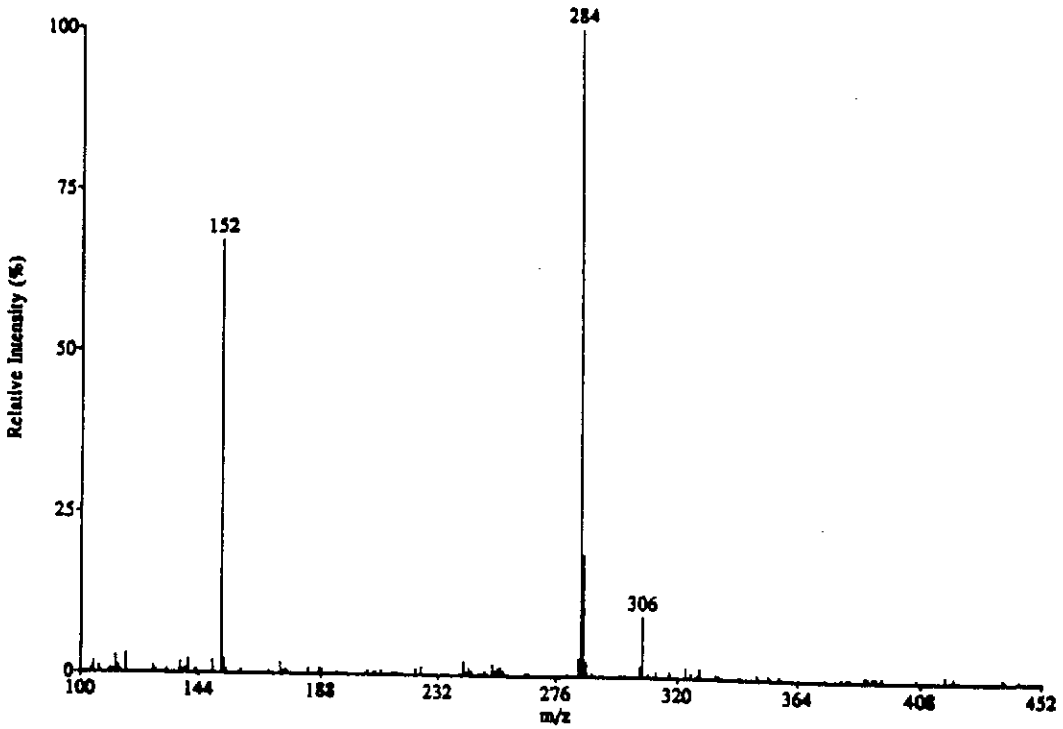

Figure 25. Positive - ion ionspray mass spectrum of 2'-deoxyadenosine (dA)

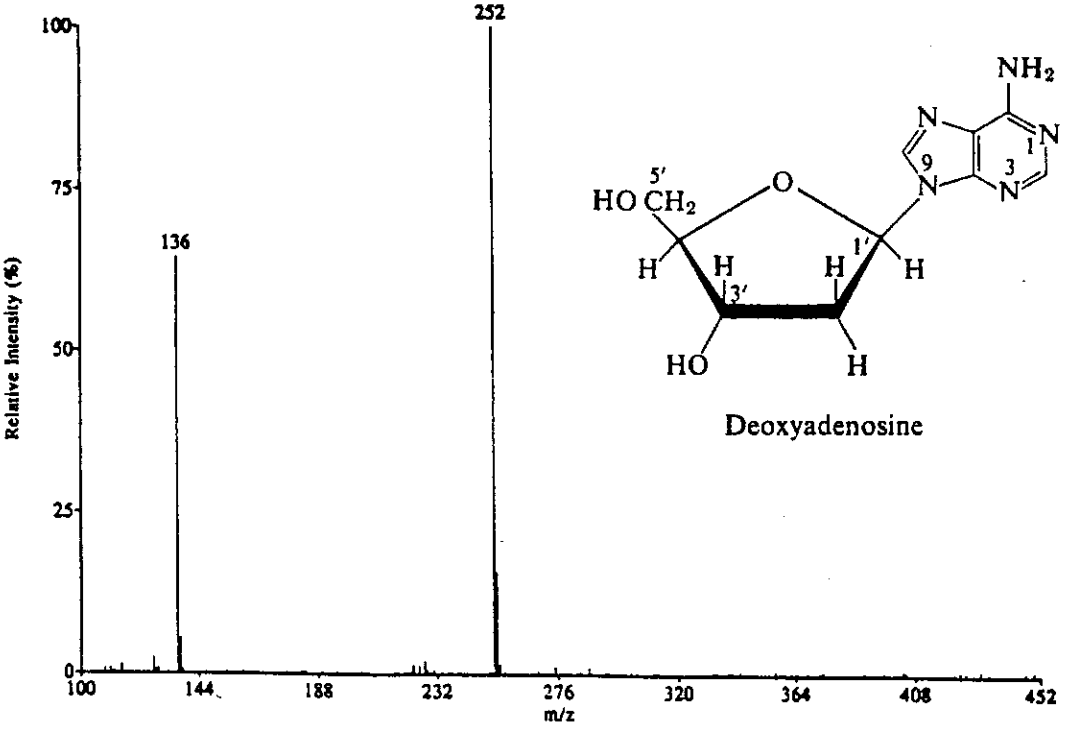

Figure 26.

Spectra for 2'- deoxyguanosine - 5' - monophosphate (pdG) and for 2'-deoxyguanosine - 3' - monophosphate (dGp).

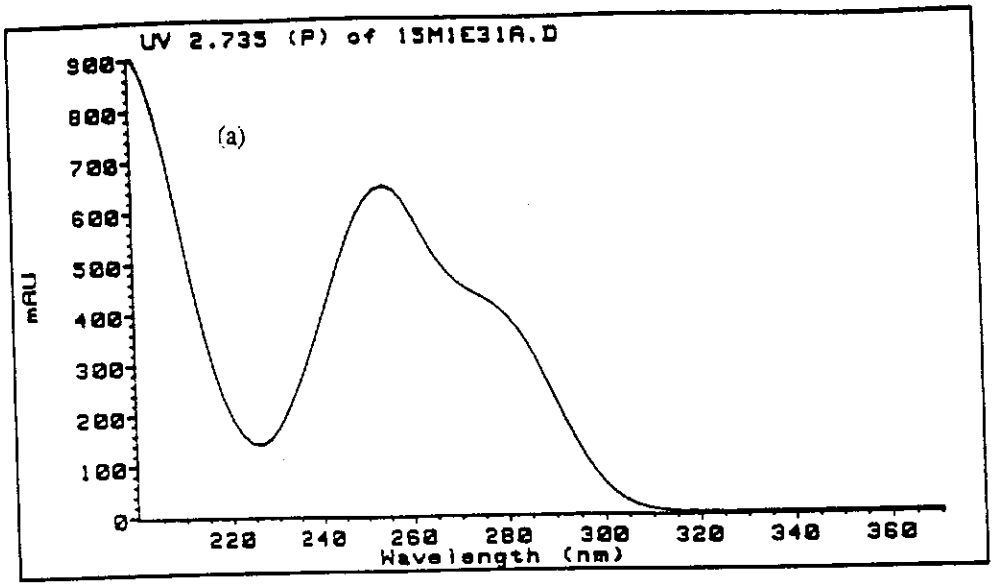

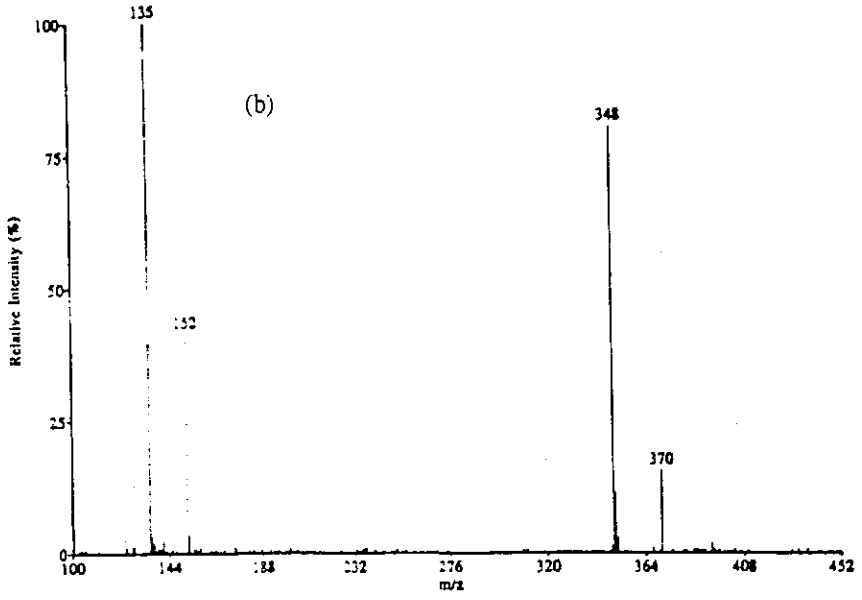

Figure 26.

Spectra for 2'- deoxyguanosine - 5' - monophosphate (pdG) and for 2'-deoxyguanosine - 3' - monophosphate (dGp).

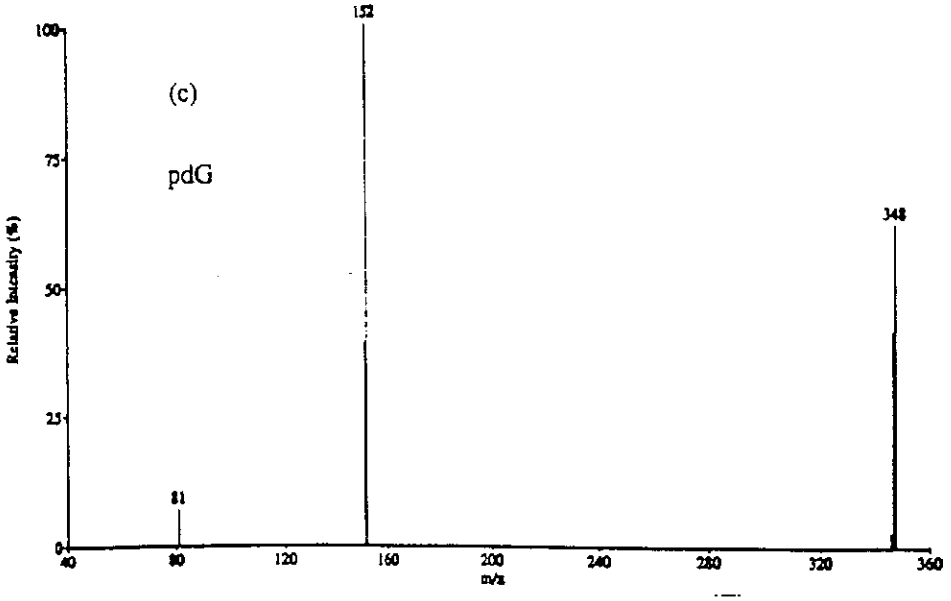

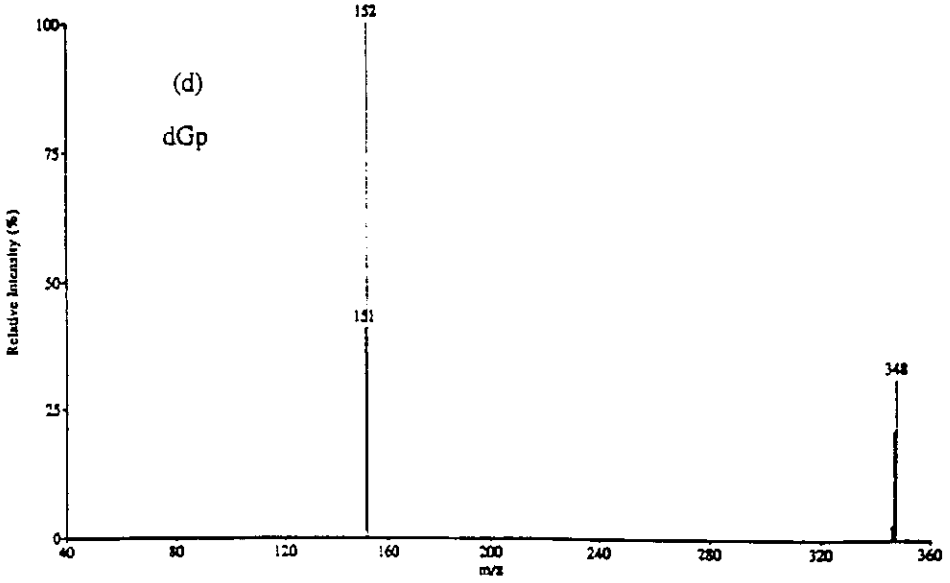

Figure 27. Fragment ion spectrum of protonated N2-isobutyryl - 2' - deoxyguanosine (N2 - isobutyryl - dG); $(M + H)^+$ ion at m/z 338.

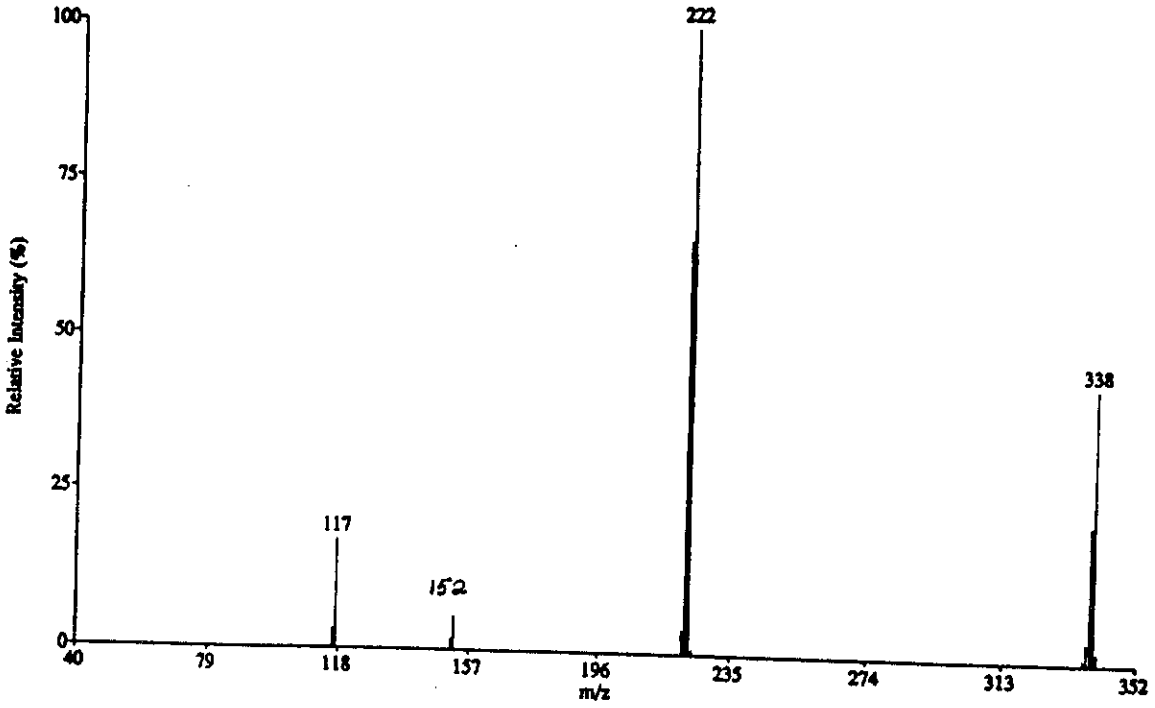

Figure 28. Fragment ion spectrum of protonated N2 - isobutyryl - 2' - deoxyguanosine - 5' - monophosphate (N2 - isobutyryl - pdG); $(M + H)^+$ ion at m/z 418.

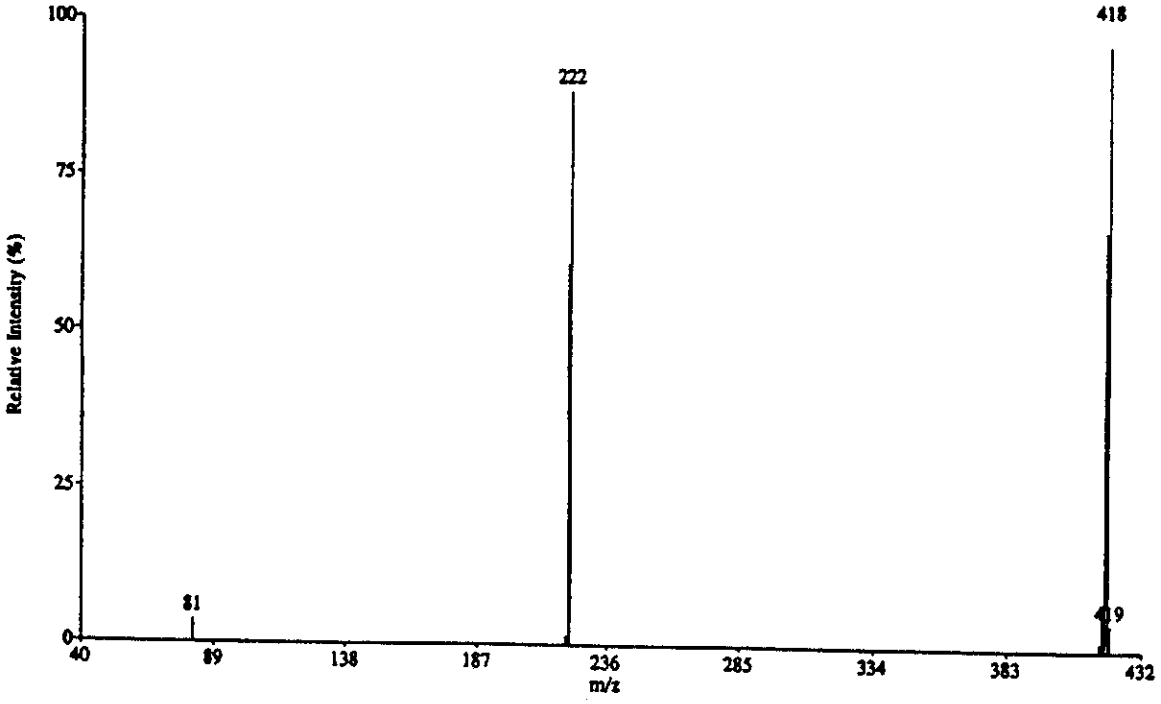

Figure 29. Positive - ion ionspray mass spectrum of the dinucleoside monophosphate 2'-deoxyadenosine - (3' - 5') - 2' - deoxycytidine (dA (3'-5') pdC)

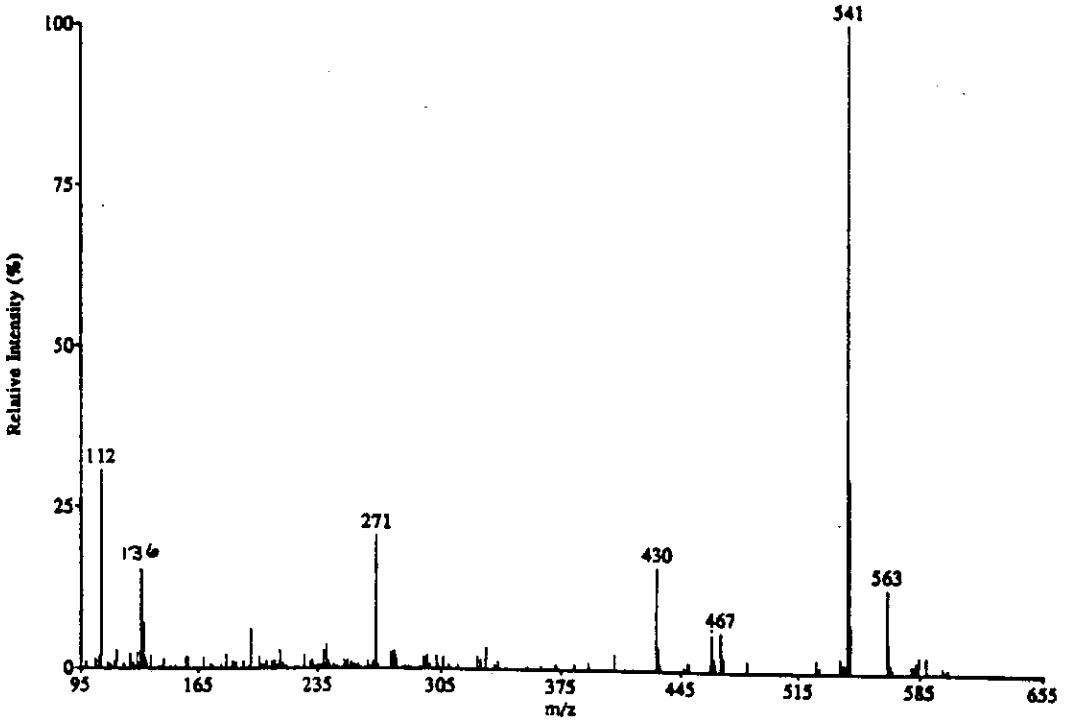

Figure 30. Positive - ion ionspray mass spectrum of the dinucleoside monophosphate, 2' - deoxyadenosine - (3' - 5') - 2' - deoxyguanosine (dA (3'-5') pdG)

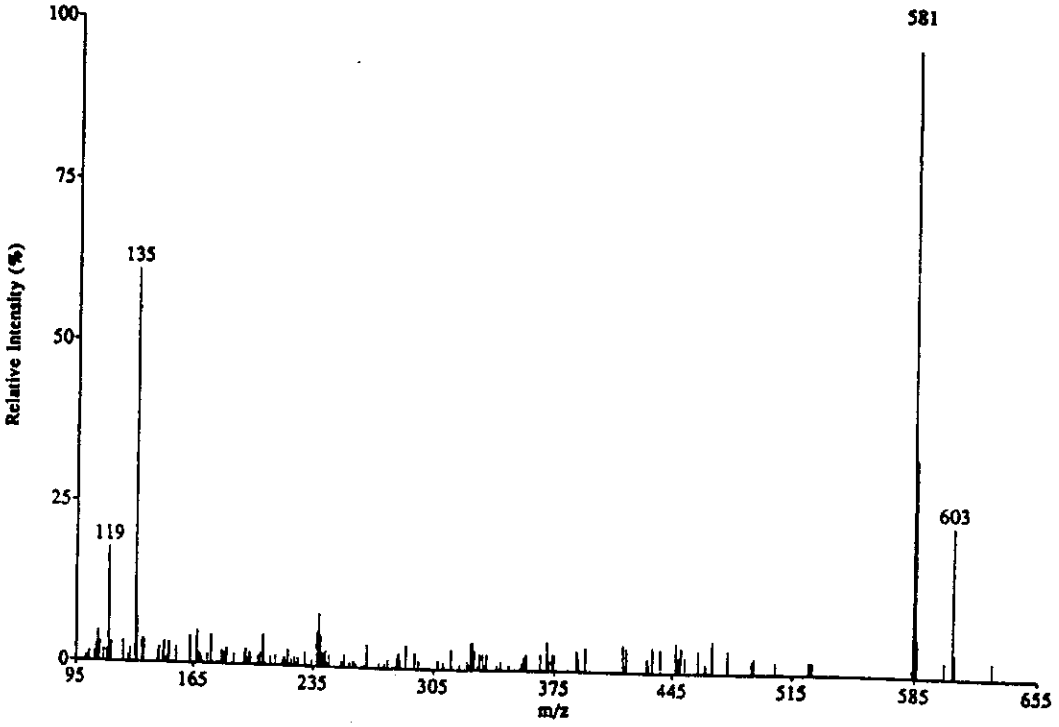

Figure 31.

Reaction scheme for N-acetoxy-2-N-acetylaminofluorene (NA-AAF) with 2'-deoxyguanosine (dG) and with 2'-deoxyguanosine -5'-monophosphate (pdG).

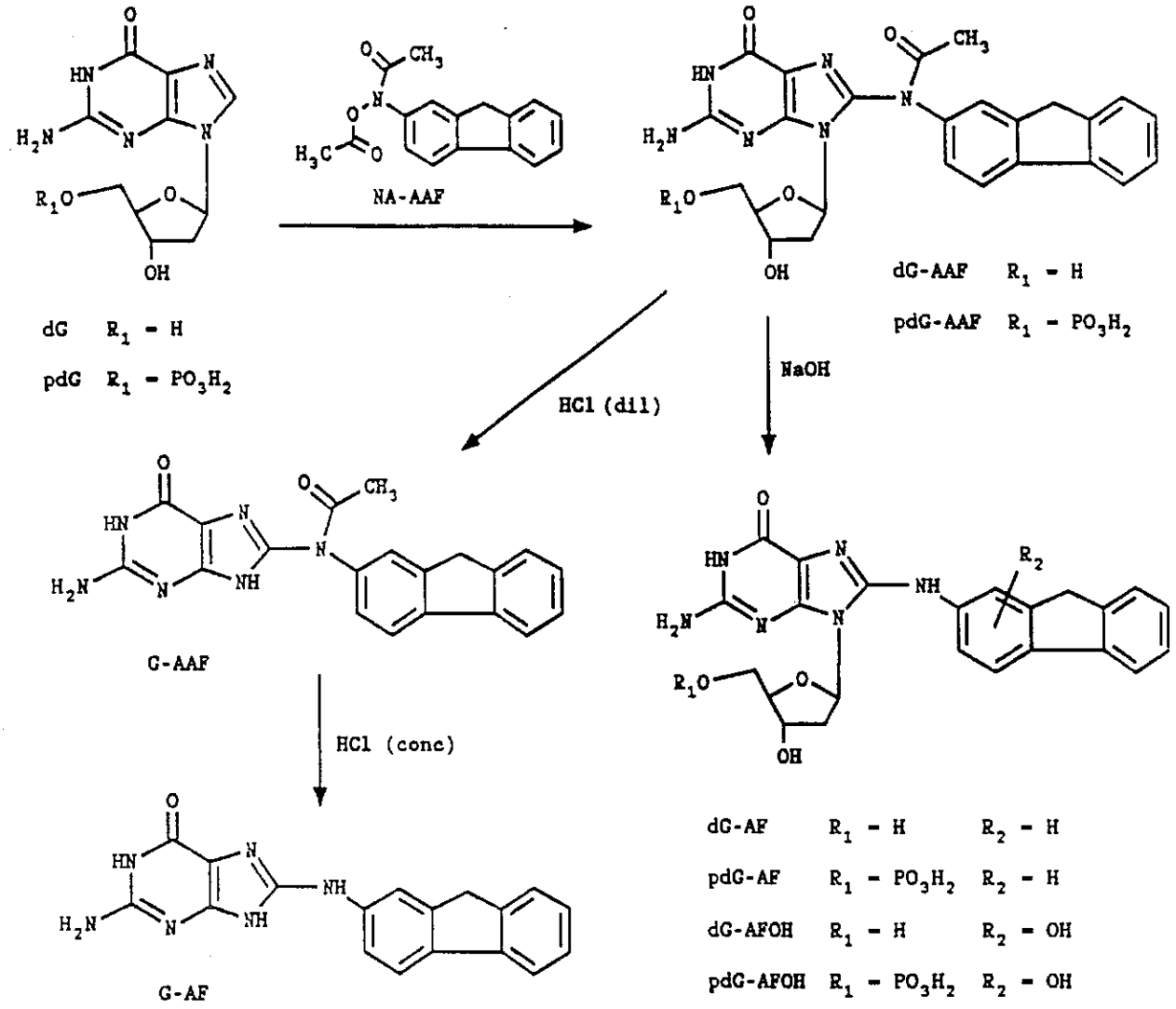

Figure 32. LC-MS analysis of reaction products resulting from reaction of NA-AAF with pdG. HPLC conditions: isocratic mobile phase, 60% methanol with 0.1% trifluoroacetic acid, 1mL/min flowrate, 4.6 mm i.d. Zorbax Rx-C8 column.

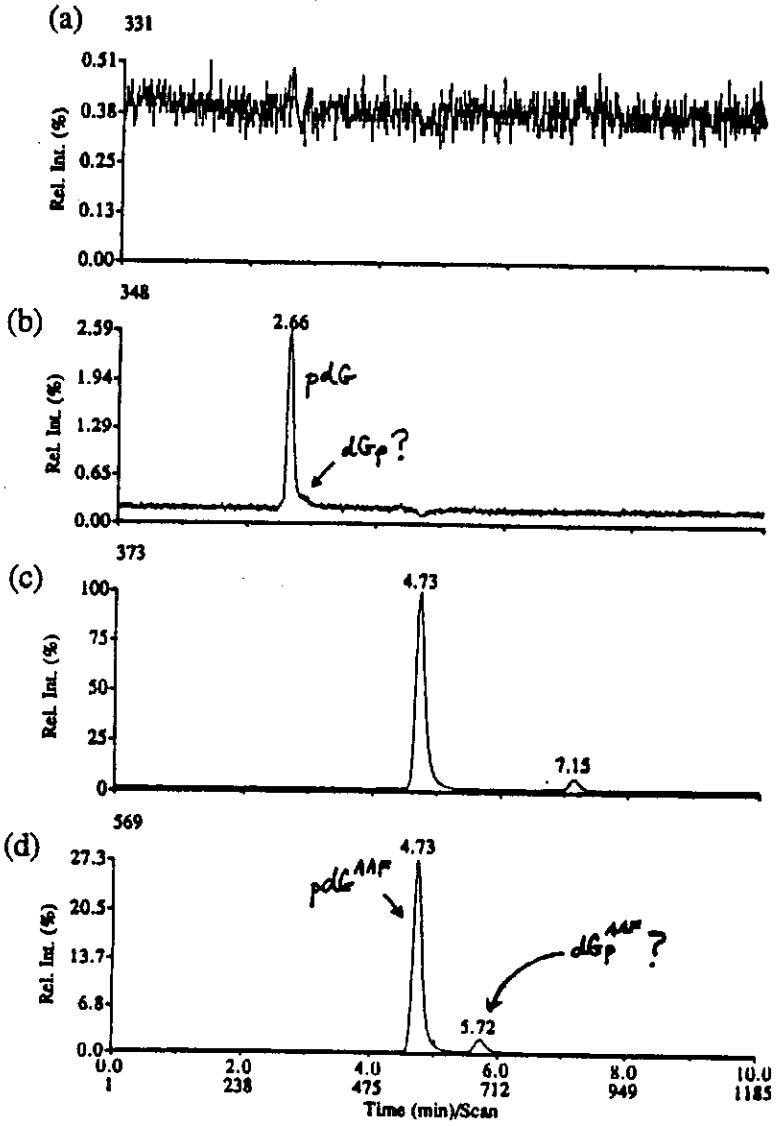

Figure 33. LC-MS analysis of reaction products resulting from reaction of NA-AAF with dG.

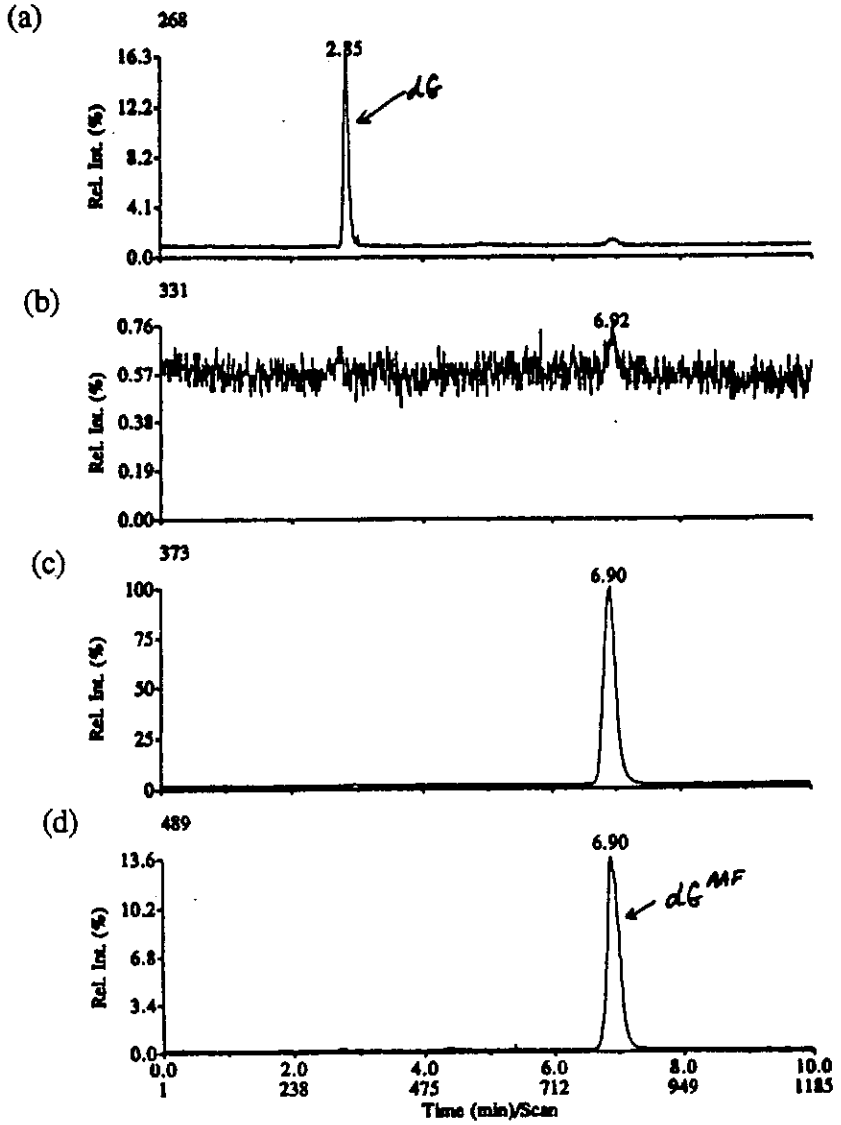

Figure 34. LC-MS analysis of reaction products resulting from hydrolysis of dG^{AAF} by dilute HCL. HPLC conditions same as for Figure 32.

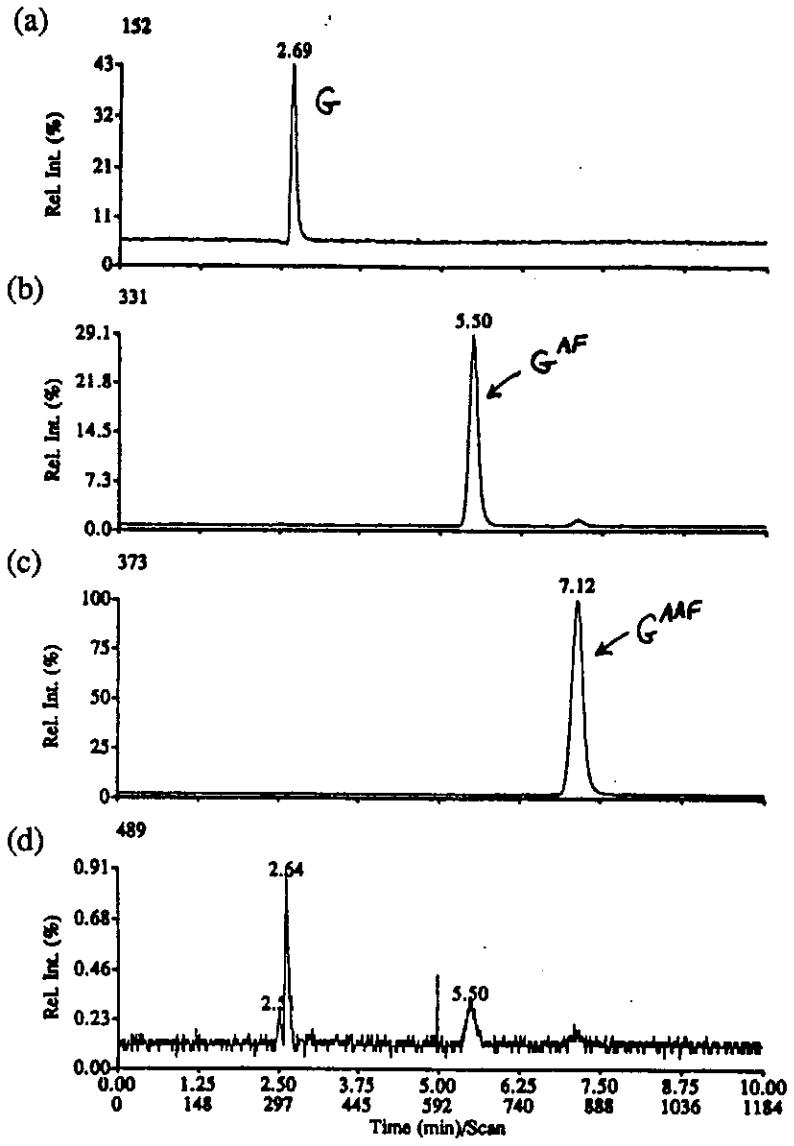

Figure 35. LC-MS analysis of reaction products resulting from hydrolysis of dG^{AAF} with concentrated HCL. HPLC conditions same as for Figure 32.

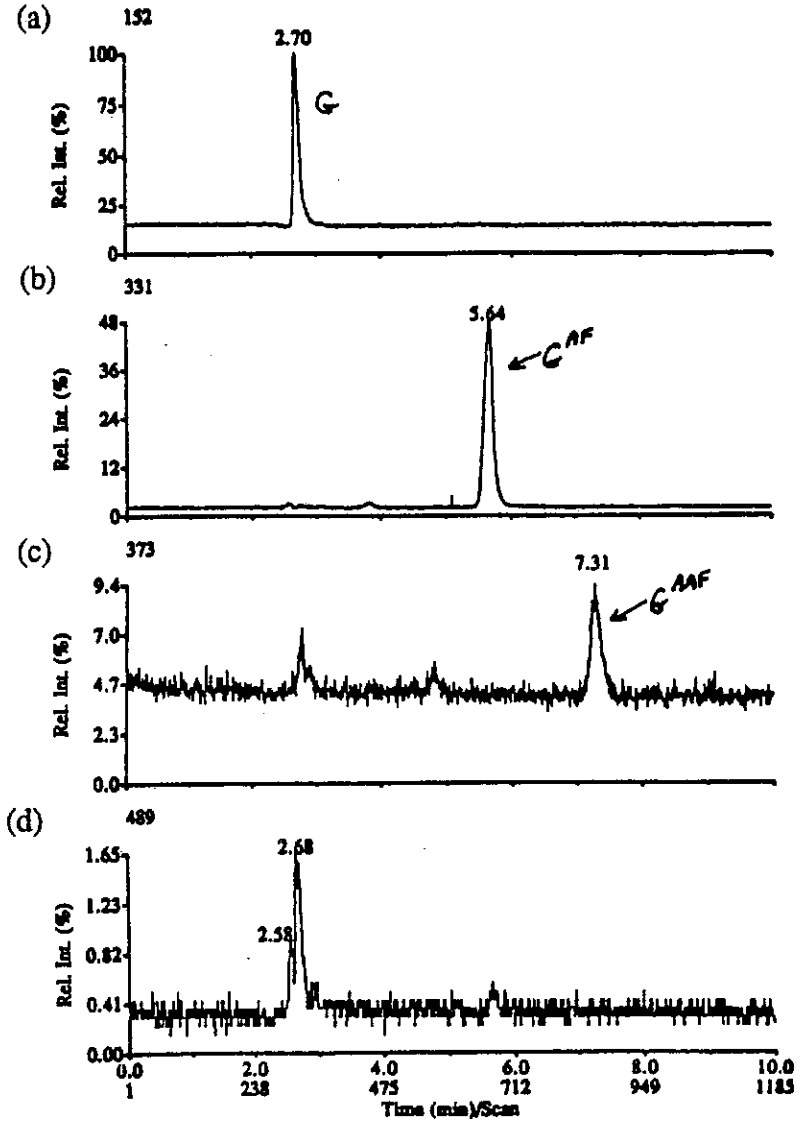

Figure 36. LC-MS analysis of reaction products resulting from hydrolysis of pdG^{AAF} with NaOH. HPLC conditions same as for Figure 32.

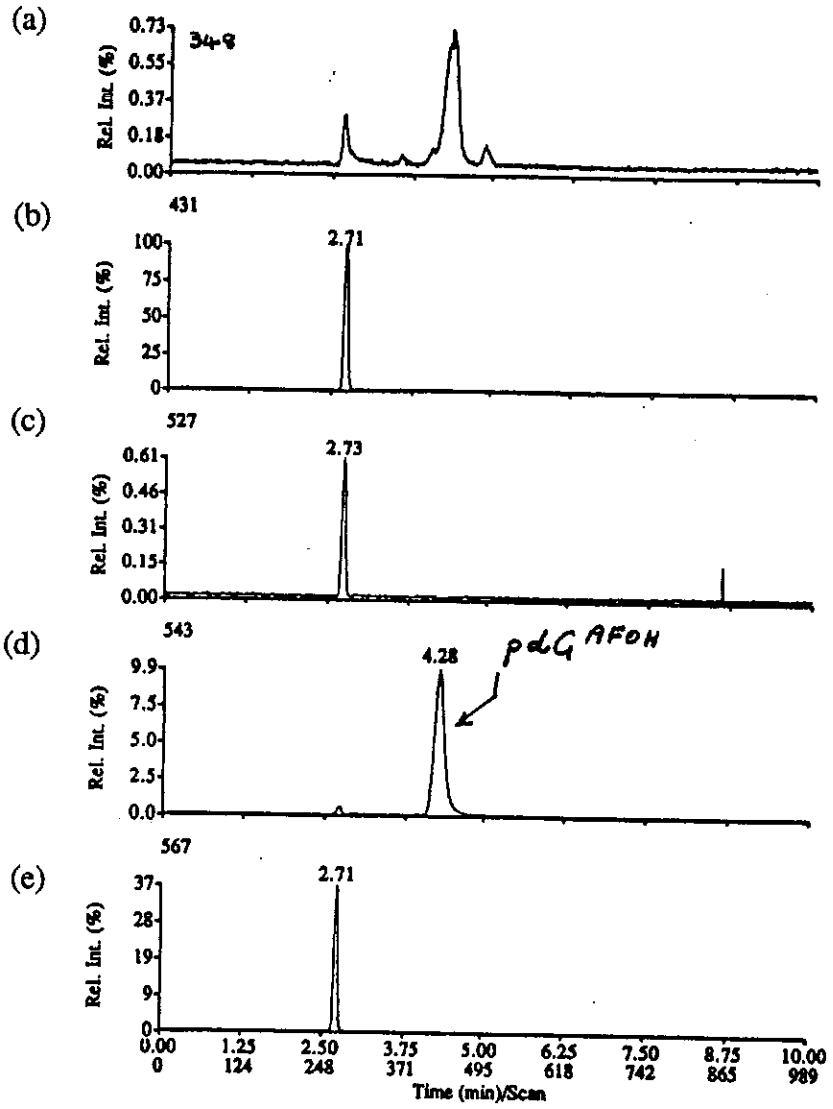

Figure 37. LC-MS analysis of reaction products resulting from hydrolysis of dG^{AAF} with NaOH. HPLC conditions same as for Figure 32.

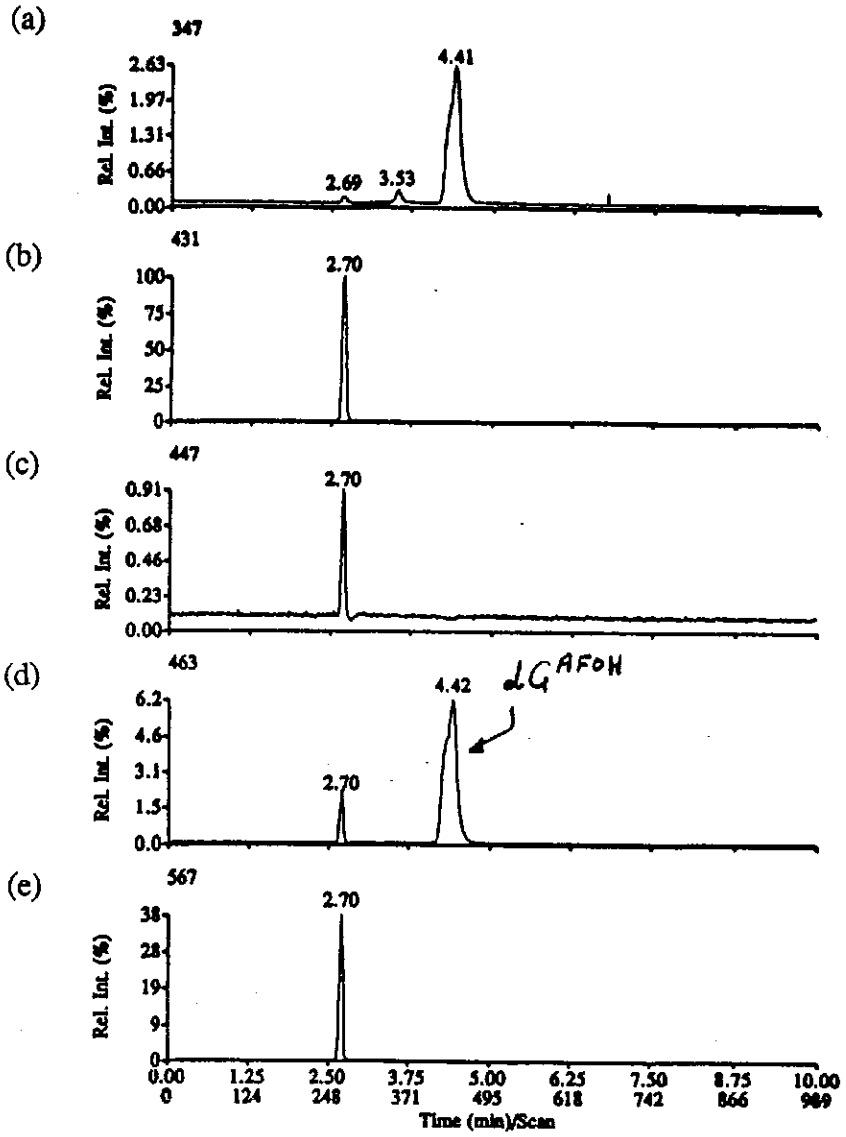

Figure 38. LC-MS analysis of same reaction mixture as in Figure 36 (Na0H hydrolysis of pdG^{AAF}) but with improved HPLC conditions (isocratic, 40% methanol, 0.1% trifluoroacetic acid).

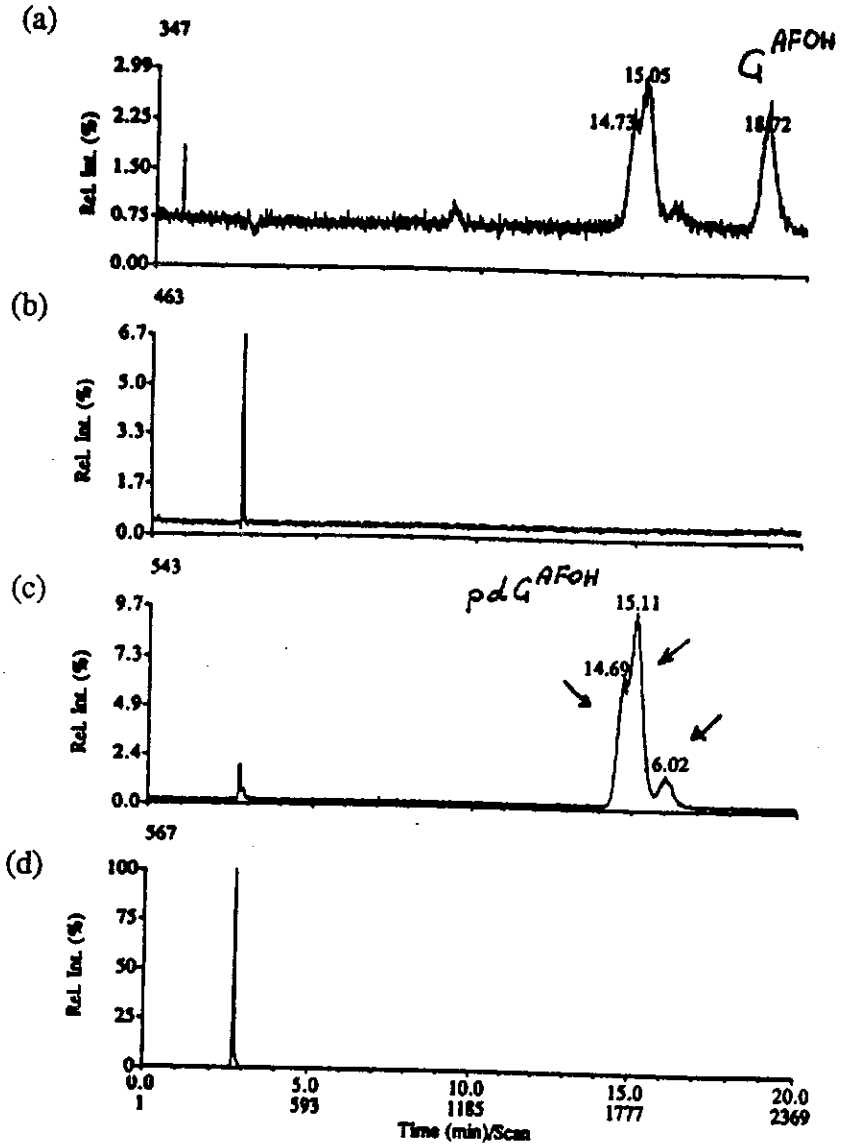

Figure 39. LC-MS analysis of same reaction mixture as in Figure 37 (NaOH hydrolysis of dG^{AAF})but with improved HPLC conditions (isocratic, 40% methanol, 0.1% trifluoroacetic acid).

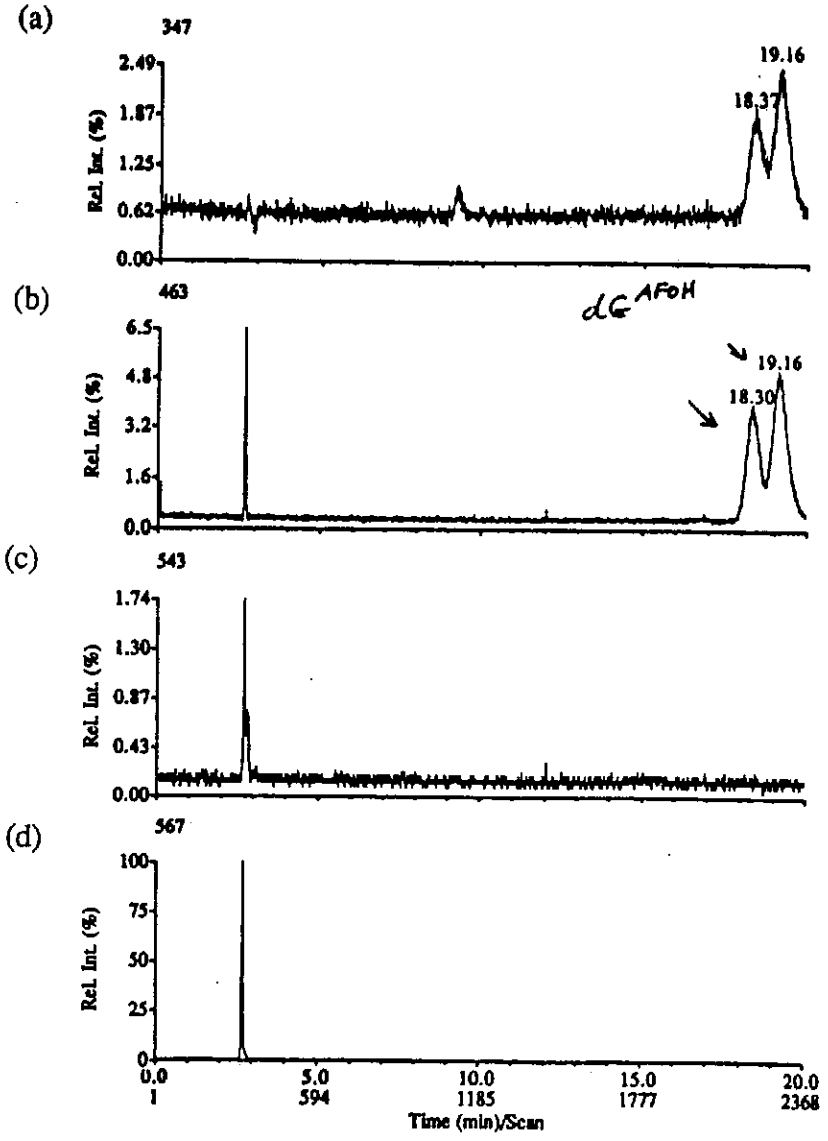

Figure 40.

Spectroscopic data for dG^{AAF} adduct. All spectra were acquired by on-line LC-UV or LC-MS experiments.

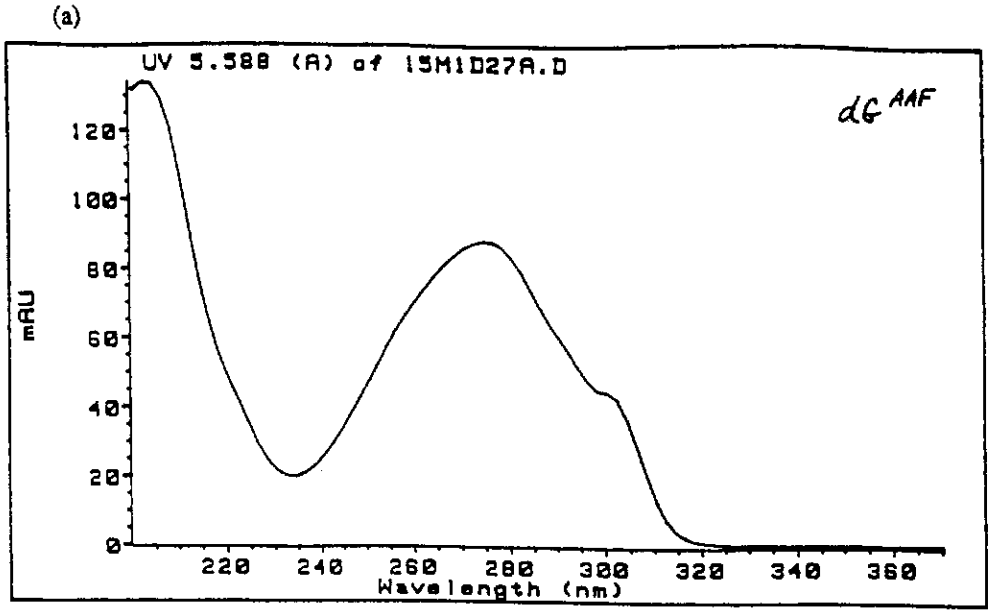

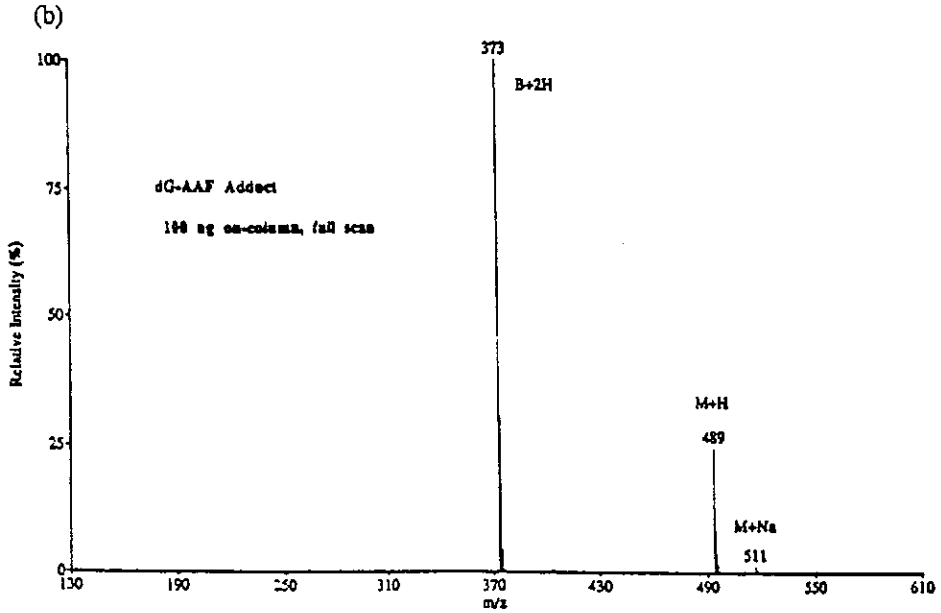

Figure 40.

Spectroscopic data for dG^{AAF} adduct. All spectra were acquired by on-line LC-UV or LC-MS experiments.

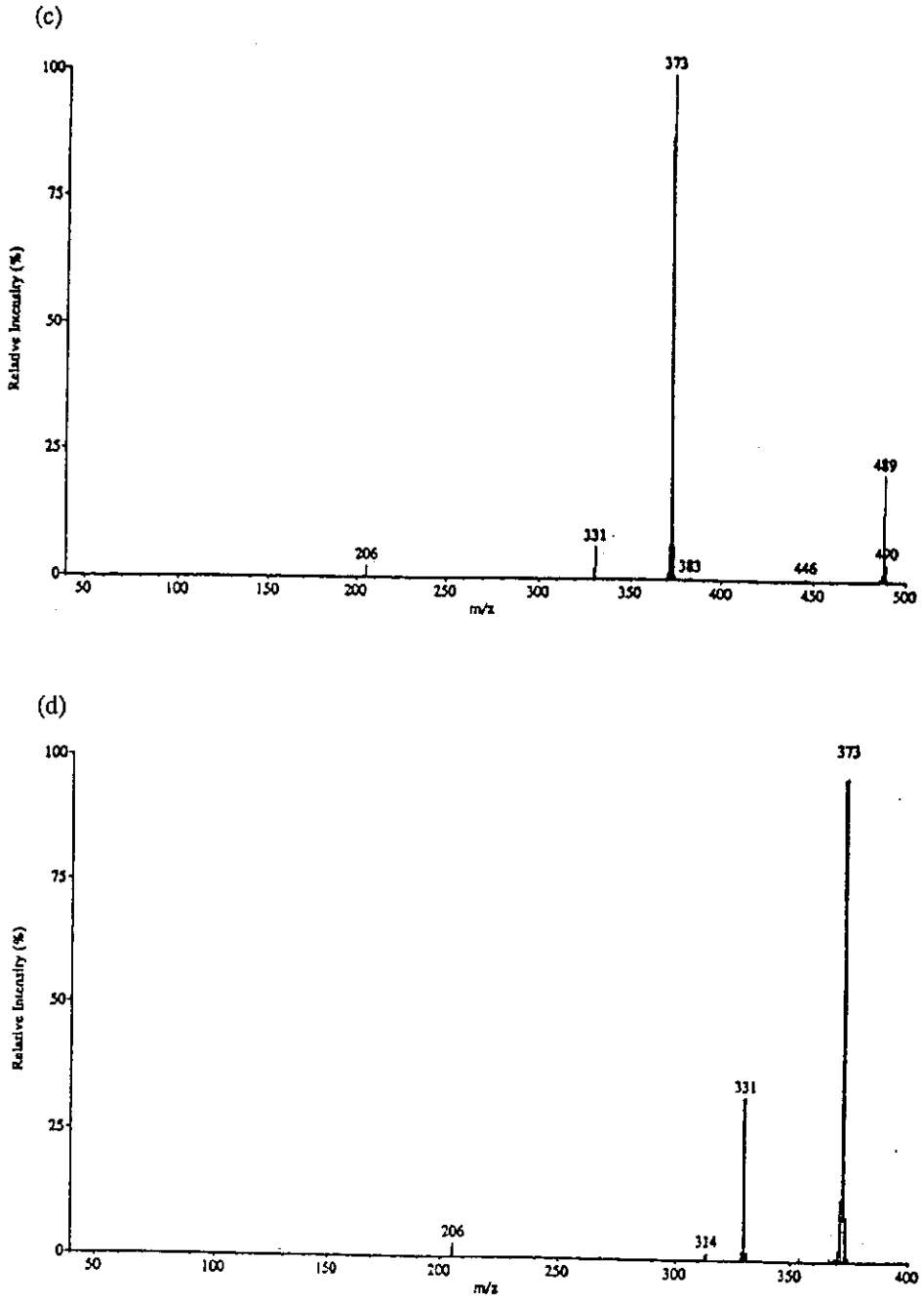

Figure 41.

Spectroscopic data for pdG^{AAF} adduct. All spectra were acquired by on-line LC-UV or LC-MS experiments.

(a)

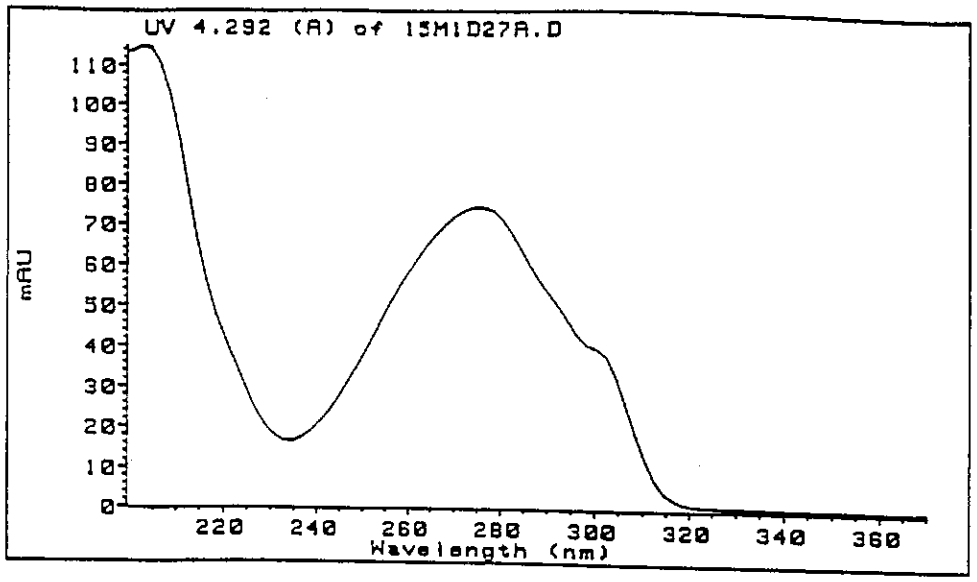

(b)

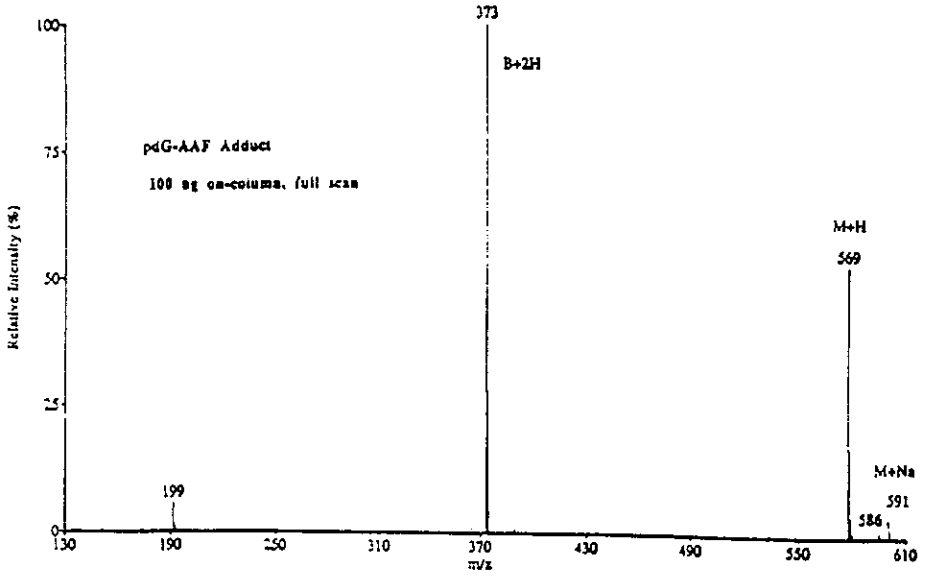

Figure 41.

Spectroscopic data for pdG^{AAF} adduct. All spectra were acquired by on-line LC-UV or LC-MS experiments.

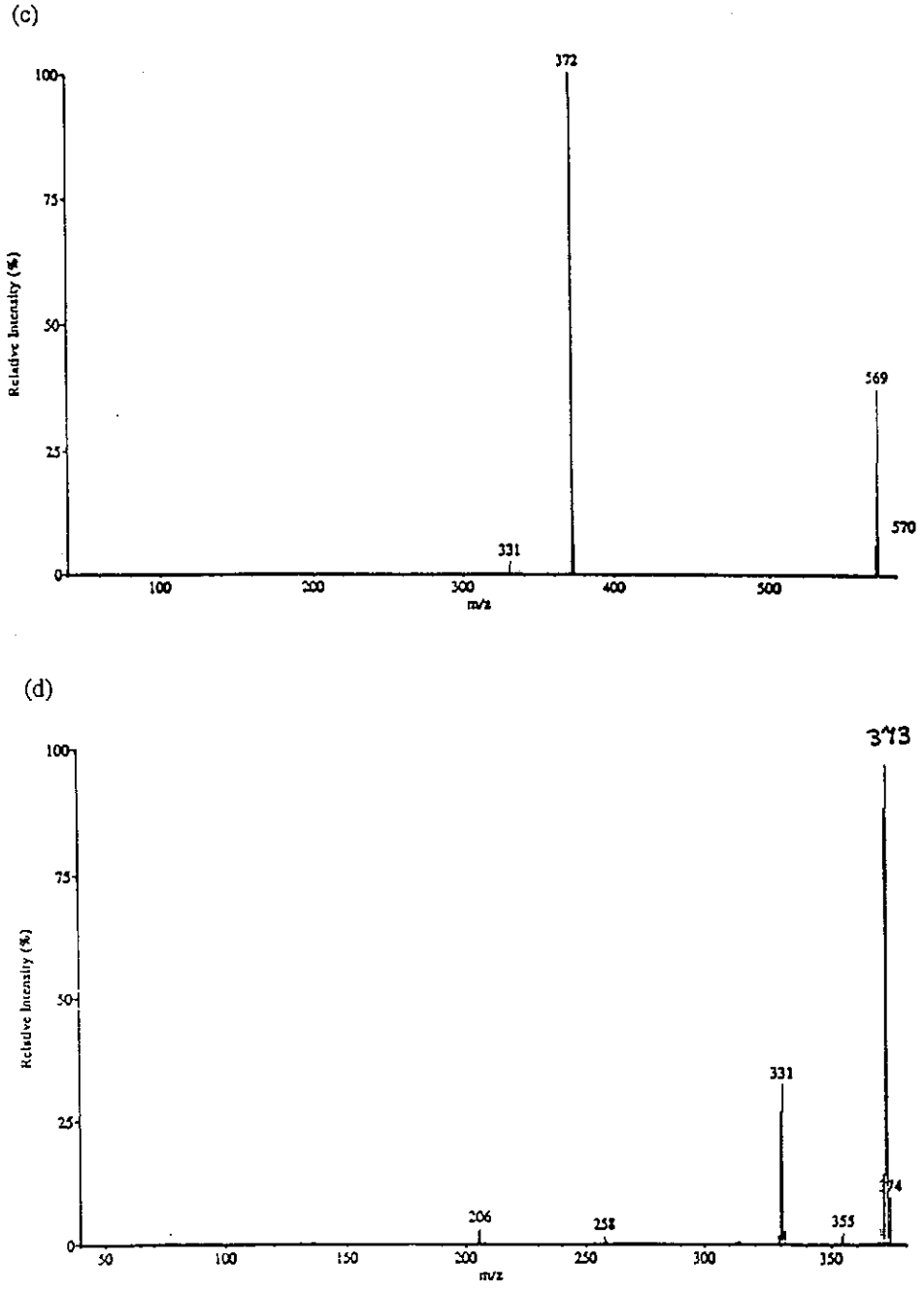

Figure 42.

Spectroscopic data for G^{AAF} adduct. Both spectra were acquired by on-line LC-UV or LC-MS experiments.

(a)

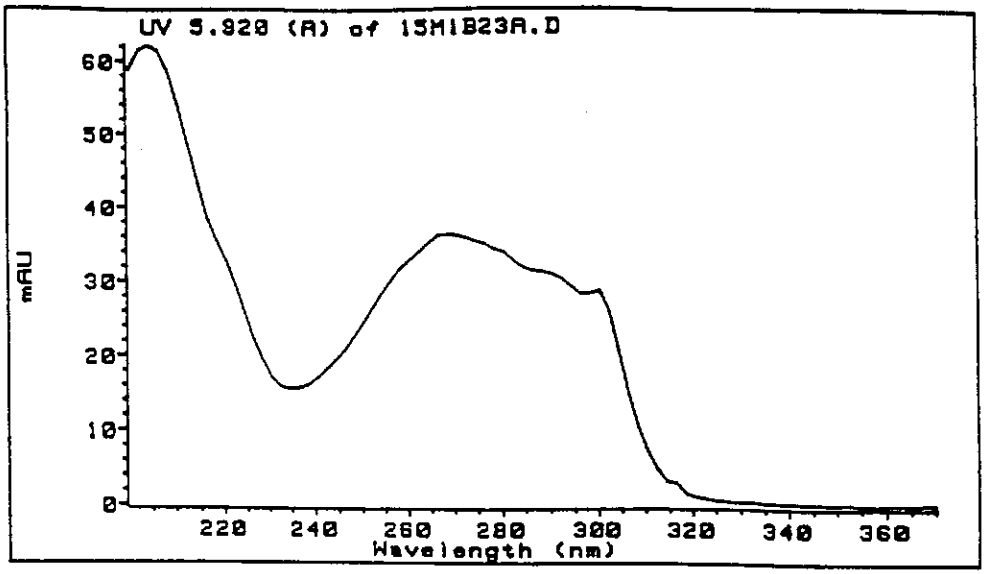

(b)

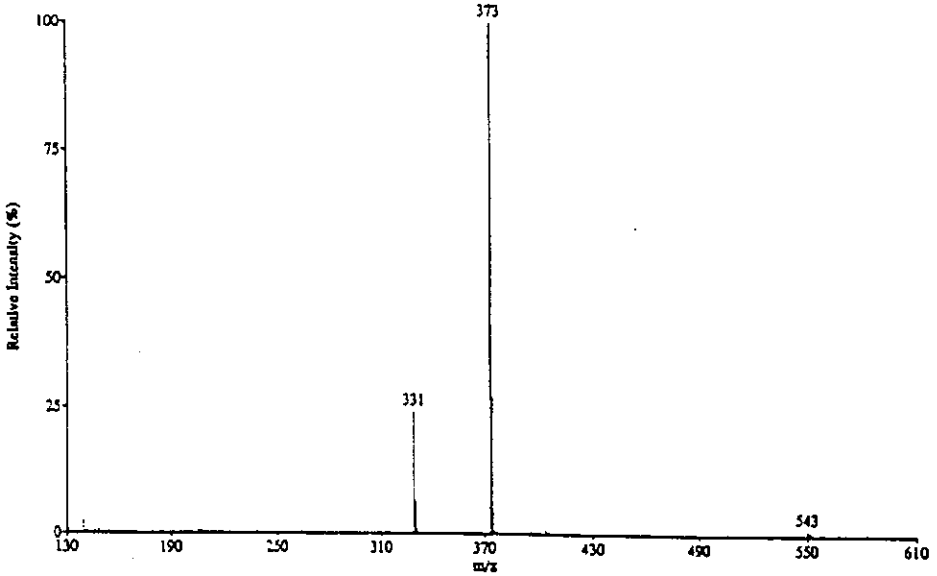

Figure 43.

Spectroscopic data for G^{AF} adduct. All spectra were acquired by on-line LC-UV or LC-MS experiments.

(a)

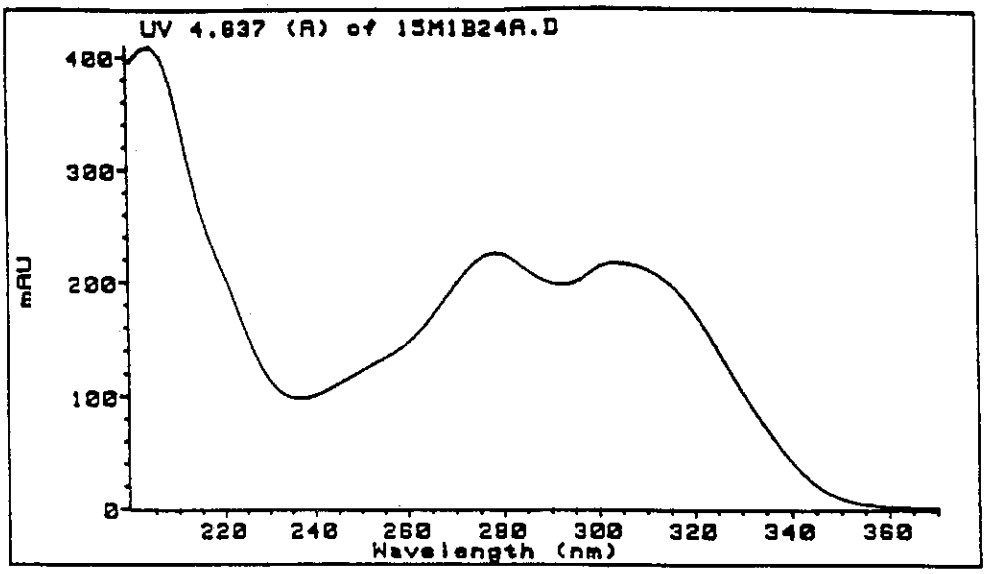

(b)

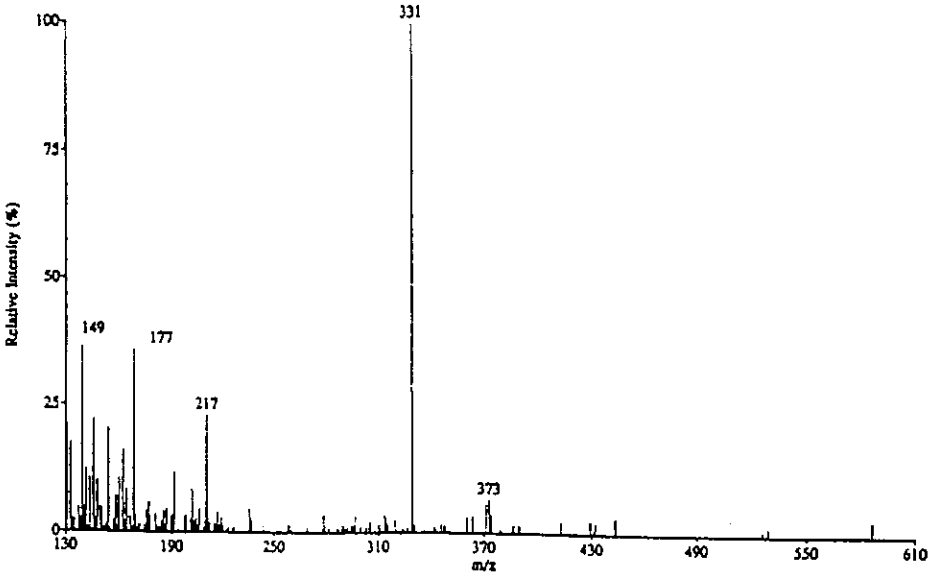

Figure 44.

Spectroscopic data for G^{APOH} adduct. Both spectra were acquired by on-line LC-UV or LC-MS experiments.

(a)

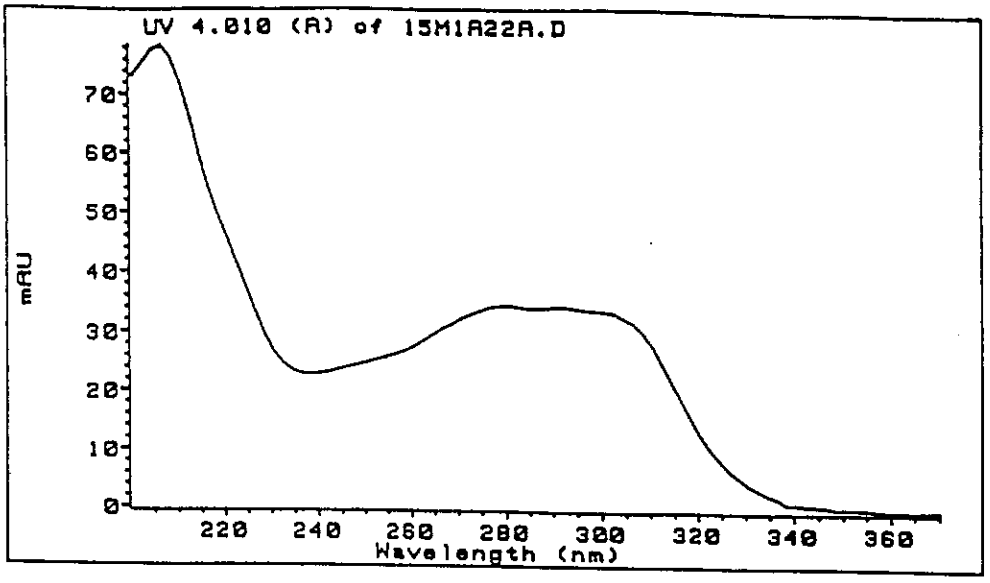

(b)

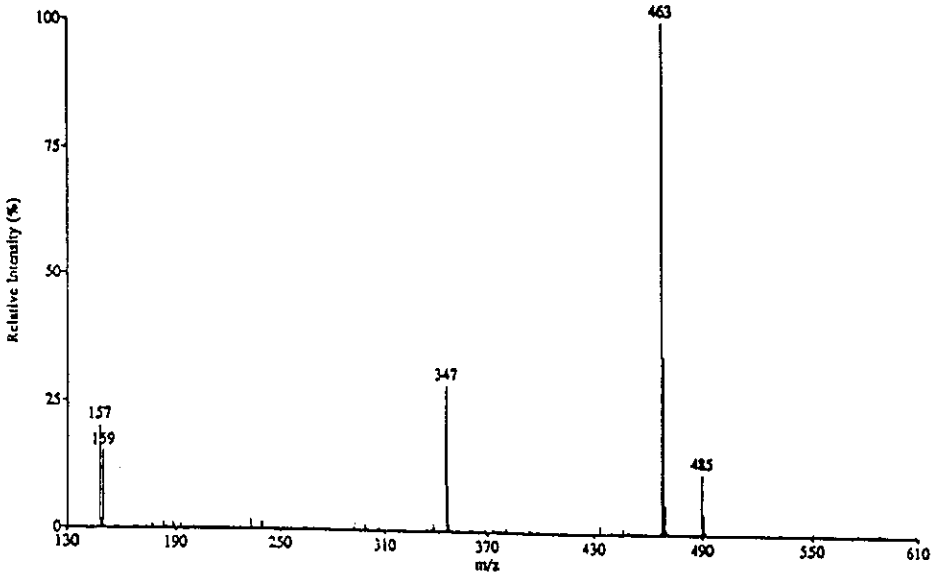

Figure 45.

Spectroscopic data for pdG$^{A\text{POH}}$ adduct. All spectra were acquired by on-line LC-UV or LC-MS experiments.

(a)

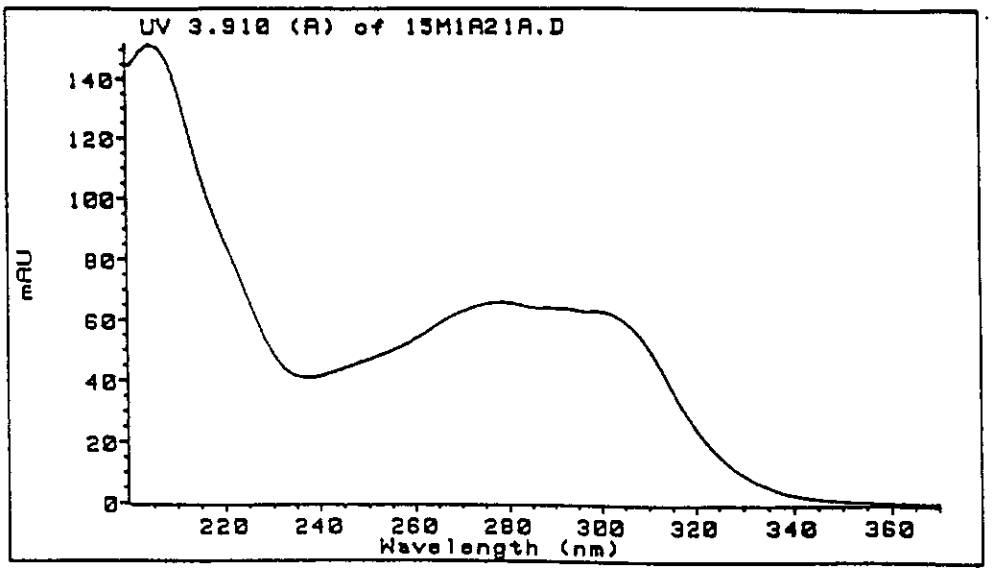

(b)

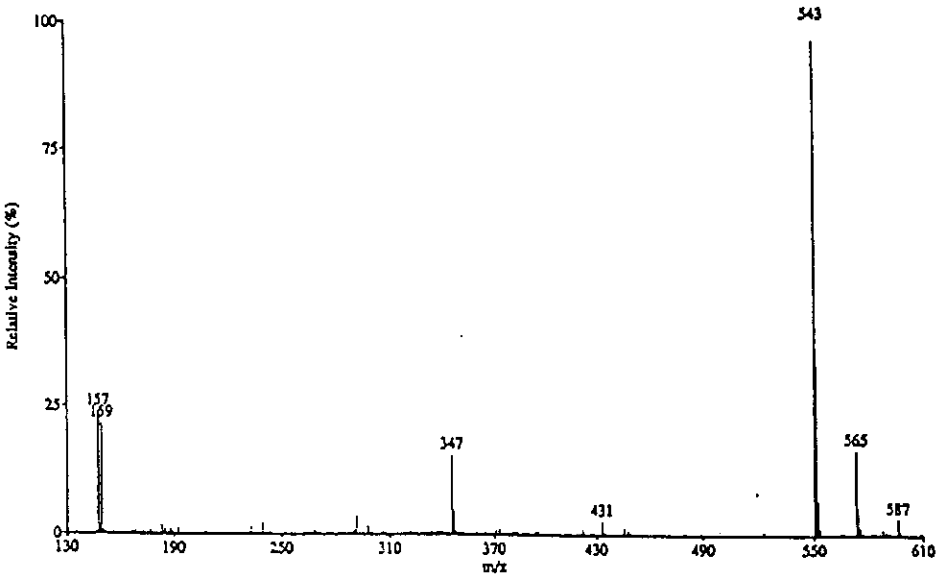

Figure 46.

LC-MS analysis of a mixture of nucleosides and nucleotides, their NA-AAF adducts and the hydrolysis products thereof. Concentrations of the adducts were all 50μg/mL. HPLC conditions the same as for Figure 32.

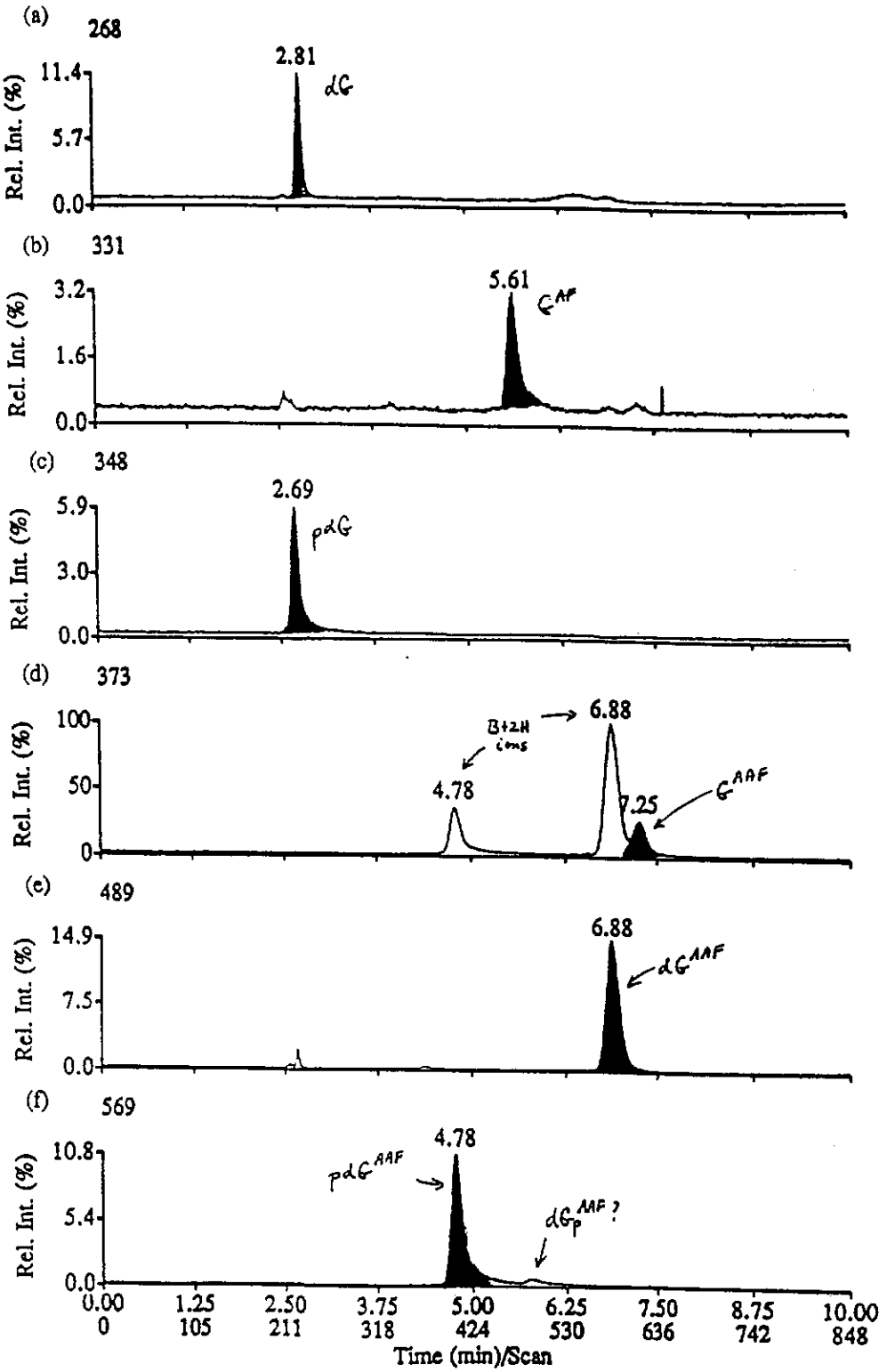

Figure 47.

Full-scan mass spectra obtained by LC-MS analysis of a mixture of dG^{AAF} and pdG^{AAF}.

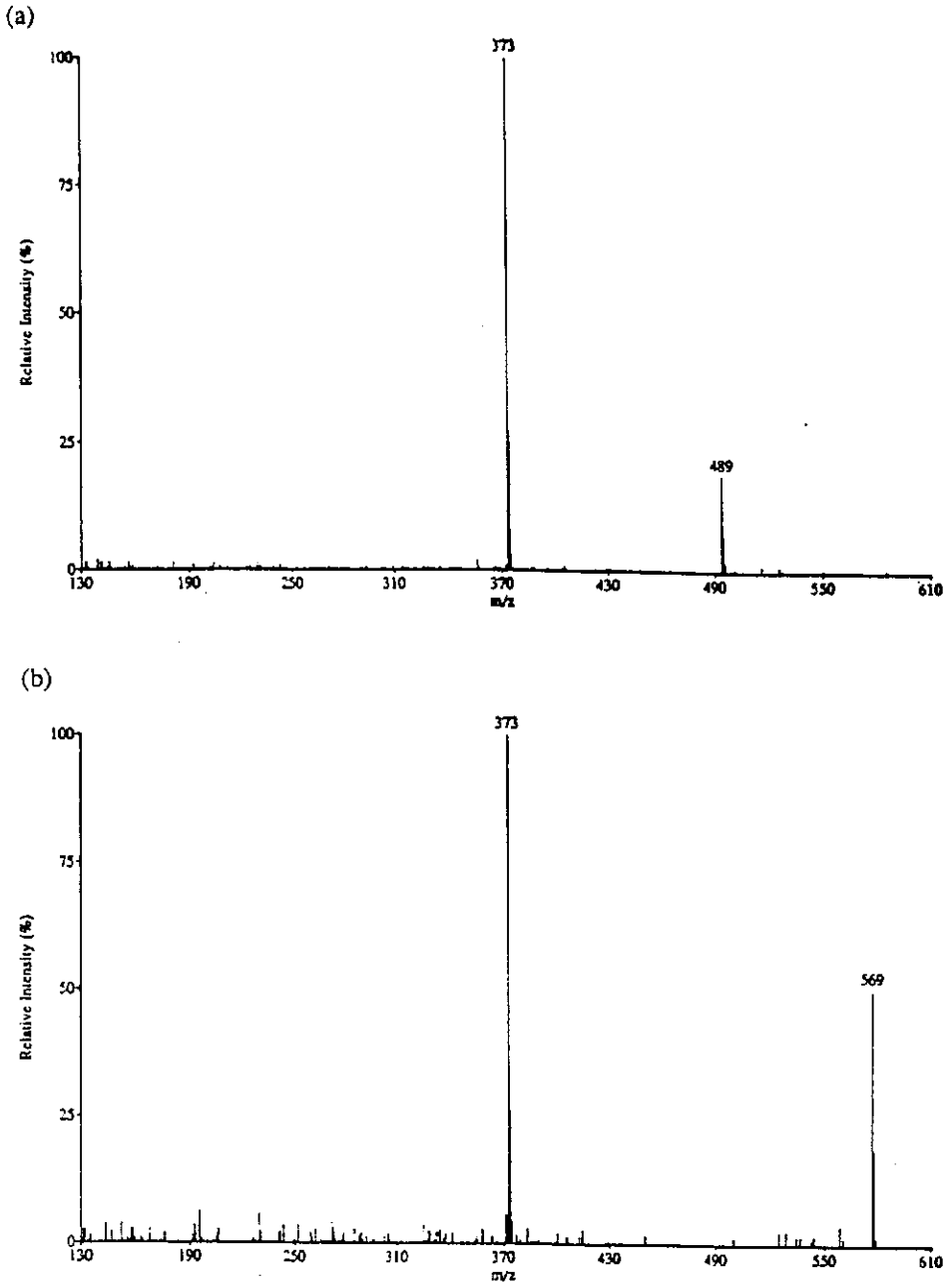

Figure 48.

Flow-injection mass spectrometric analysis, using selected ion monitoring, of a mixture of purified adducts dG^{AAF} and pdG^{AAF}. Amounts injected are indicated. Ions monitored include the $(M + H)^+$ ions of each adduct (m/z 489 and 569 for dG^{AAF} and pdG^{AAF}, respectively) and m/z 373 which corresponds to protonated G^{AAF} formed as a fragment ion of each of the two adducts injected. The bottom three traces are identical to the top three, but expanded by a factor of 32.

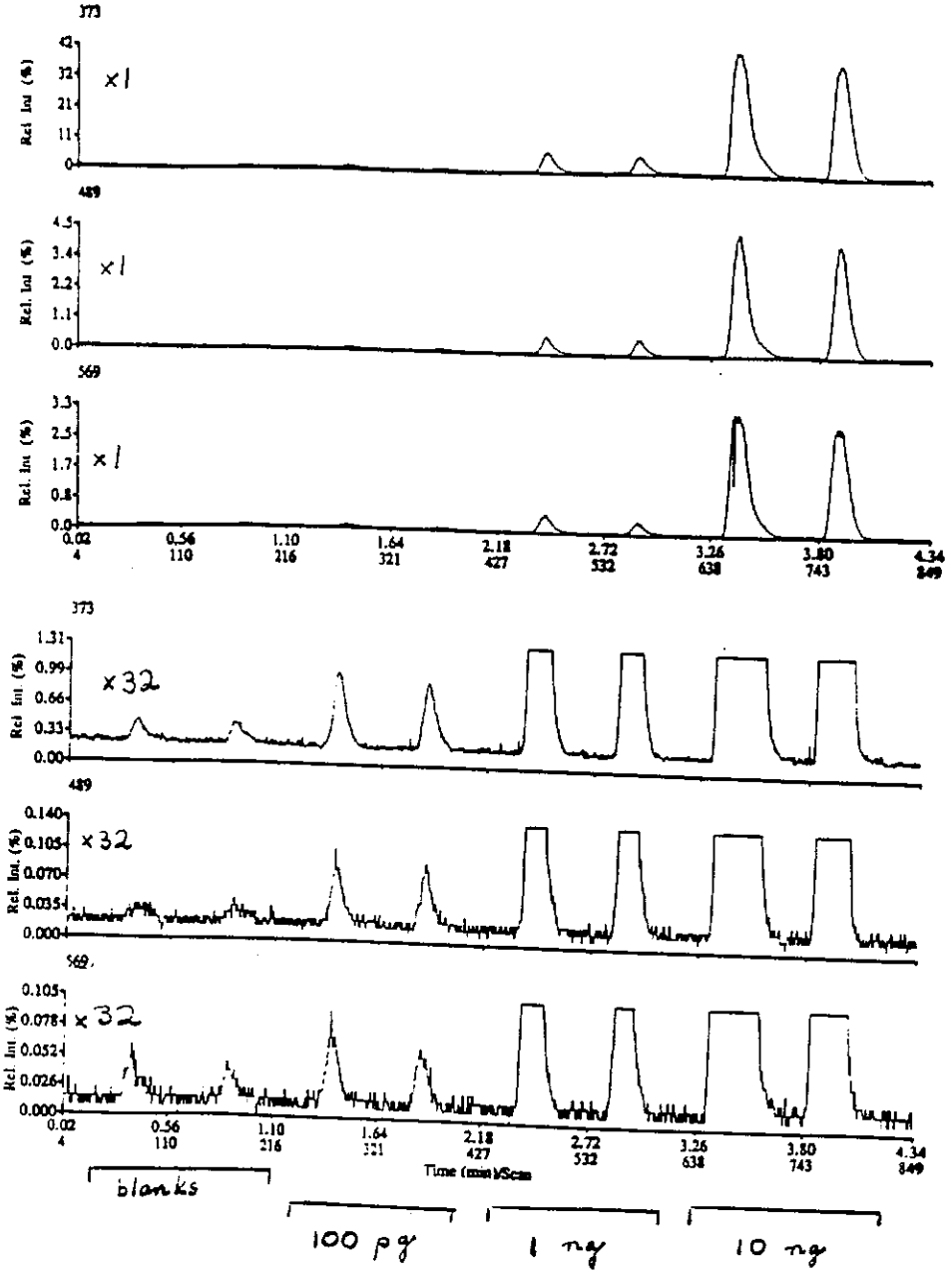

Figure 49.

LC-MS analysis of a mixture of pdG (250 µg/mL) plus the adducts pdG^{AAF} and dG^{AAF} (each 250 ng/mL). HPLC conditions same as for Figure 32; post-column split of 1:20 (mass spectrometer : waste), 5µL injected on-column.